

# eRNA profiling uncovers the enhancer landscape of oesophageal adenocarcinoma and reveals new deregulated pathways

Ibrahim Ahmed, Shen-Hsi Yang, Samuel Ogden, Wei Zhang, Yaoyong Li, The OCCAMs consortium, Andrew D Sharrocks\*

School of Biological Sciences, Faculty of Biology, Medicine and Health, University of Manchester, Manchester, United Kingdom

**Abstract** Cancer is driven by both genetic and epigenetic changes that impact on gene expression profiles and the resulting tumourigenic phenotype. Enhancers are transcriptional regulatory elements that are key to our understanding of how this rewiring of gene expression is achieved in cancer cells. Here, we have harnessed the power of RNA-seq data from hundreds of patients with oesophageal adenocarcinoma (OAC) or its precursor state Barrett's oesophagus coupled with open chromatin maps to identify potential enhancer RNAs and their associated enhancer regions in this cancer. We identify ~1000 OAC-specific enhancers and use these data to uncover new cellular pathways that are operational in OAC. Among these are enhancers for *JUP*, *MYBL2*, and *CCNE1*, and we show that their activity is required for cancer cell viability. We also demonstrate the clinical utility of our dataset for identifying disease stage and patient prognosis. Our data therefore identify an important set of regulatory elements that enhance our molecular understanding of OAC and point to potential new therapeutic directions.

\*For correspondence:  
andrew.d.sharrocks@manchester.ac.uk

Competing interest: See page 20

Funding: See page 20

Preprinted: 11 May 2022

Received: 06 June 2022

Accepted: 20 February 2023

Published: 20 February 2023

Reviewing Editor: William C Hahn, Dana-Farber Cancer Institute, United States

© Copyright Ahmed *et al.* This article is distributed under the terms of the [Creative Commons Attribution License](#), which permits unrestricted use and redistribution provided that the original author and source are credited.

## Editor's evaluation

This is an important study that identifies enhancer-associated (e)RNAs specifically associated with Oesophageal adenocarcinoma (OAC). Integrative analyses of patient gene expression data and epigenetic data from an OAC-derived cell line provide convincing support for the identification of eRNAs as markers of enhancers that are important for OAC tumour biology. This paper should be of wide general interest to researchers interested in how epigenetics drive cancer development.

## Introduction

Enhancers are distal regulatory elements that generally promote gene expression by engaging with the promoters of their target genes in cis (*Andersson and Sandelin, 2020*), although they have also been observed acting in trans (*Hu et al., 2008; Spilianakis et al., 2005*) and more recently, through hubs of activity on extra-chromosomal DNA species (*Hung et al., 2021*). Active enhancers are characterised by the presence of histone marks such as H3K27ac and H3K4me1 (*Creyghton et al., 2010; Heintzman et al., 2007*). However, it has been shown that enhancers can be the site of production for small transcripts termed enhancer RNAs (eRNAs) (*De Santa et al., 2010; Kim et al., 2010*). Whilst the functionality of eRNAs is still under debate, there is a large body of evidence associating the production of eRNAs with enhancer activity, and subsequent target gene activation (*Tyssowski et al., 2018; Andersson et al., 2014; Chen et al., 2018*). This association with gene expression has allowed

eRNA-defined enhancer activity to serve as a specific marker for developmental stage and tissue type (Yan *et al.*, 2019; Huang *et al.*, 2016). Furthermore, eRNAs provide molecular markers for disease, often with more sensitivity than the gene expression pattern itself (Zhang *et al.*, 2019; Chen *et al.*, 2018).

During tumorigenesis, there are widespread changes to gene expression patterns that are associated with rewiring of the regulatory landscape in an enhancer-driven manner (Li *et al.*, 2015; Hsieh *et al.*, 2014). This can be accompanied by eRNA production. For example, production of an eRNA from the PSA gene enhancer is associated with increased PSA expression in castration-resistant prostate cancer (Zhao *et al.*, 2016). This potentially makes the production of eRNAs a biomarker for cancer, but this is widely underappreciated. Indeed, a recent pan cancer study demonstrated that eRNAs can serve as prognostic markers across various cancer types and provide novel insights into cancer biology (Chen *et al.*, 2018), leading to the identification of therapeutic opportunities.

Oesophageal adenocarcinoma (OAC) has an overall 5-year survival rate of approximately 15%, making it a leading global cause of cancer-associated deaths (Coleman *et al.*, 2018). OAC is believed to arise in a stepwise fashion from the pre-cancerous lesion Barrett's oesophagus (BO) (Peters *et al.*, 2019). A number of large-scale DNA sequencing studies have been performed into the pathogenesis of OAC from Barrett's (Frankell *et al.*, 2019; Ross-Innes *et al.*, 2015; Stachler *et al.*, 2015), however there is still uncertainty concerning the precise molecular mechanisms. In an effort to understand potential epigenetic contributors to OAC, we have previously demonstrated that changes in chromatin accessibility play a role in the transition to OAC (Britton *et al.*, 2017; Rogerson *et al.*, 2019; Rogerson *et al.*, 2020). These chromatin changes are often associated with non-coding regions of the genome that may represent regulatory elements such as enhancers.

Here, we build on our previous work identifying chromatin changes during the BO to OAC transition (Britton *et al.*, 2017; Rogerson *et al.*, 2019; Rogerson *et al.*, 2020). By integrating total RNA-seq data from BO and OAC patients generated by the Oesophageal Cancer Clinical and Molecular Stratification (OCCAMS) consortium dataset, with previously generated chromatin accessibility data on these tissues (Britton *et al.*, 2017; Rogerson *et al.*, 2019; Rogerson *et al.*, 2020; Corces *et al.*, 2018), we identify, and validate, pervasive eRNA production at regions of accessible chromatin, indicative of enhancer activity. Subsequent interrogation of genes associated with these enhancers identified deregulated pathways of importance and demonstrated the potential clinical utility of eRNA profiling in OAC.

## Results

### Identification of potential intergenic eRNA transcripts in OAC patients

eRNAs are generally unstable and lowly abundant, making them hard to detect in RNA-seq datasets. We therefore harnessed the sequencing power derived from combining hundreds of patient samples to discover potential eRNAs (Figure 1A). To identify eRNAs that are relevant to OAC we interrogated RNA-seq data generated from 210 OAC patients and also from 108 Barrett's patients to identify differentially upregulated eRNAs in OAC (Jammula *et al.*, 2020). After mapping sequencing reads to the genome, we excluded all regions corresponding to gene bodies as well as sequences 2 kb upstream from the transcriptional start site (TSS) and 500 bp downstream from the annotated transcriptional termination site (TTS) (Figure 1—figure supplement 1A) to avoid interference from promoter sequences and read through transcription, respectively. Next, we identified all of the accessible regions of chromatin in OAC and Barrett's samples within this truncated genome by creating a union peak set from ATAC-seq performed on 14 OAC and 4 Barrett's samples (Britton *et al.*, 2017; Rogerson *et al.*, 2019; Rogerson *et al.*, 2020; Corces *et al.*, 2018) (resulting in 150,265 peaks). To focus on potential enhancer regions, we then took the RNA-seq data from both classes of patients and assessed raw reads within these accessible chromatin regions. This identified 61,349 intergenic regions that contain RNA transcripts and represent potential eRNA regions. We then filtered these based on a read count  $\geq 3$  and fragments per million (FPM) value  $\geq 1.5$ , which resulted in a final high-confidence set of 4600 potential eRNA containing enhancer regions in OAC and Barrett's patients (Supplementary file 1).

Next, we identified differentially transcribed eRNAs in each disease state ( $\pm > 0.5 \log_2$  fold;  $p_{\text{ue}_{\text{adj}}} < 0.05$ ; Figure 1B) and found 959 to be significantly upregulated in OAC (Supplementary file 2)

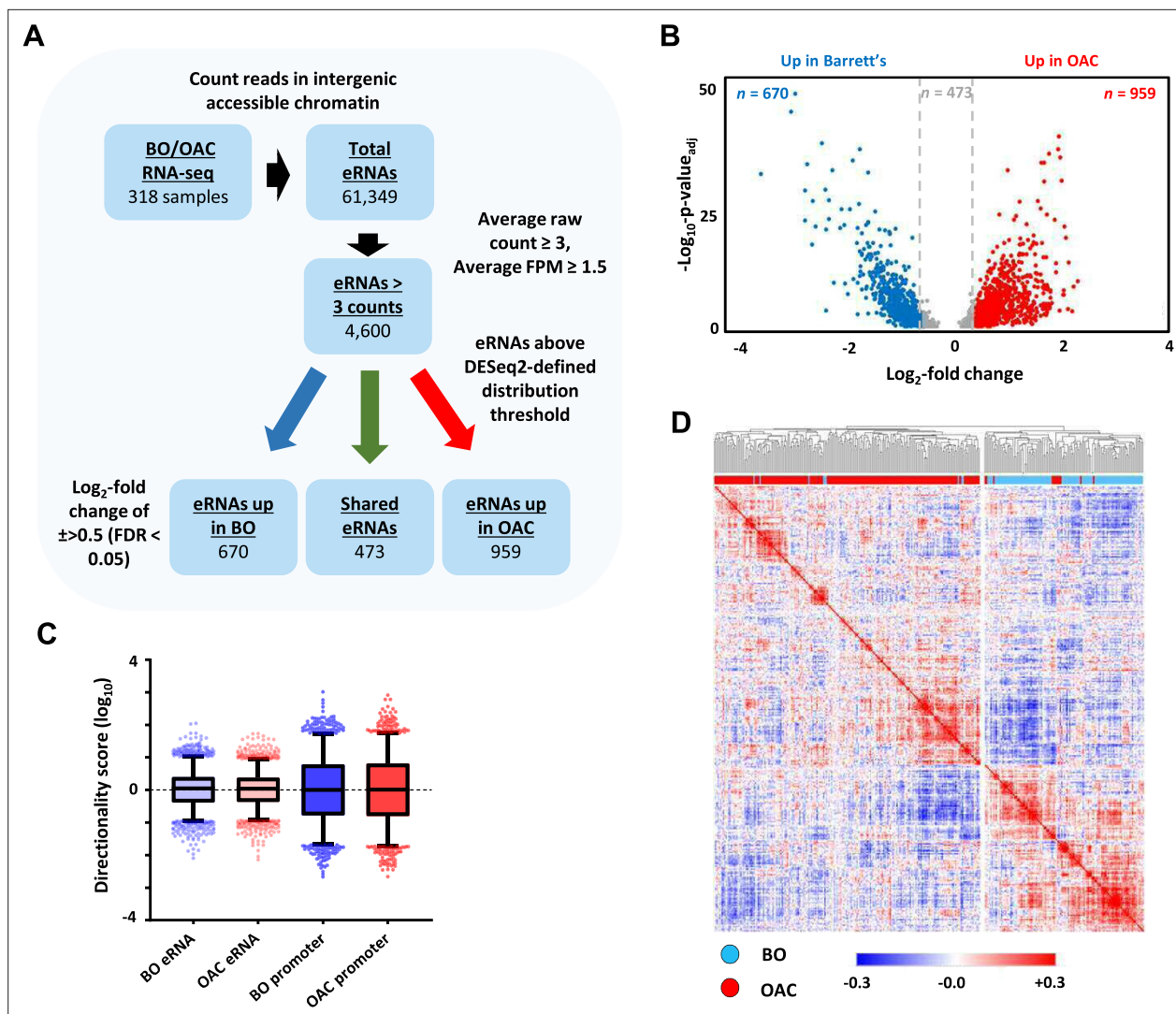


**Figure 1.** Identification of enhancer transcription in oesophageal adenocarcinoma (OAC) and Barrett's patients. **(A)** Enhancer RNA (eRNA) identification strategy. The numbers of putative eRNAs identified at each stage are indicated. **(B)** Volcano plot displaying the differentially expressed ( $\pm \text{Log}_2\text{FC} > 0.5, p_{\text{adj}} < 0.05$ ) eRNAs ( $n = 2102$ ). **(C)** Directionality scores for Barrett's oesophagus (BO)- or OAC-specific eRNAs compared to promoters. **(D)** Pearson's correlation and hierarchical clustering of BO ( $n = 108$ ) and OAC ( $n = 210$ ) patient tissue total RNA-seq samples according to row z-score normalised expression levels in the 4600 eRNA regions. See also **Figure 1—figure supplement 1**.

The online version of this article includes the following figure supplement(s) for figure 1:

**Figure supplement 1.** Identification of enhancer transcription in Barrett's oesophagus (BO) and oesophageal adenocarcinoma (OAC) patients.

and 670 to be more active in Barrett's patients (**Supplementary file 3**). 2498 eRNAs did not meet the stringent DESeq2 distribution threshold and were discarded. The remaining putative eRNAs exhibited low directionality score distributions consistent with the bidirectional transcription associated with eRNA production (**Figure 1C**; **Figure 1—figure supplement 1B**).

To probe the clinical utility of eRNA region profiling, we analysed the expression levels found in the 4600 eRNA regions across all of the OAC and Barrett's samples. Hierarchical clustering showed a clear separation of Barrett's and OAC patients (**Figure 1D**). While clustering based on whole RNA-seq data gave broadly similar separation of OAC and Barrett's samples, several more were misclassified compared to eRNA-based profiling (**Figure 1—figure supplement 1C**; 37 vs. 8 samples). Clustering of the expression of the same eRNA regions in a different RNA-seq dataset (**Maag et al., 2017**) also provided a good separation of the OAC and Barrett's samples (**Figure 1—figure supplement 1D**), further demonstrating the relevance of this dataset. In summary therefore, we have identified a panel

of potential eRNA generating regions that can be used for discriminating OAC samples from the pre-cancerous Barrett's state.

### eRNA-associated regions show enhancer-like characteristics

Having identified a group of accessible chromatin regions expressing potential eRNAs, we next sought further evidence to associate these with enhancer-like activity. First, we examined chromatin accessibility in OAC patients and found higher levels at eRNA expressing loci compared to a random set of open chromatin regions (**Figure 2A**; left). Furthermore, these regions also exhibited higher levels of the H3K27ac chromatin mark in OE19 OAC-derived cells that is usually associated with active enhancers (**Figure 2A**; right). This was not just a function of increased accessibility as a control group of more highly accessible regions did not exhibit increased levels of H3K27ac (**Figure 2—figure supplement 1A**). Indeed, chromatin accessibility levels are a weak indicator of eRNA transcription levels across patient samples, as even regions of greater accessibility contained much lower transcript levels (**Figure 2B**; **Figure 2—figure supplement 1B**). Thus, eRNA regions are more accessible but the reciprocal is not true, as more accessible regions do not necessarily show higher levels of eRNA transcription.

To provide further evidence for association with active enhancers in OAC cells, we used CUT&Tag (**Kaya-Okur et al., 2020**) to profile a range of histone marks and chromatin-associated proteins in OE19 cells and correlated the levels of these across the eRNA expressing regions (**Figure 2C**). There is clear co-association with a range of enhancer-associated marks and proteins, including RNA polymerase II, BRD4, and the MED1 subunit of mediator. This is also evident when visualising the data as heatmaps compared to random regions of accessible chromatin, where there are higher levels of the chromatin-associated marks/proteins that categorise enhancers in the eRNA regions (**Figure 2—figure supplement 1C**). Conversely, there is a clear depletion of the promoter-associated mark H3K4me3 (**Figure 2—figure supplement 1D**). We also examined the distribution of the chromatin marks H3K4me1 (associated with active and poised enhancers) and H3K4me3 (associated with active promoters) found in gastric adenocarcinoma (GAC) patients which are molecularly similar to OAC patients (**Cancer Genome Atlas Research Network et al., 2017**). Neither mark is enriched in the eRNA containing regions compared to random accessible regions (**Figure 2—figure supplement 1E**). However, there is a clear enrichment of H3K4me1 and depletion of H3K4me3 in eRNA containing regions compared to promoters, consistent with their designation as potential enhancers (**Figure 2—figure supplement 1F**). Conversely, the CpG content of the eRNA regions was substantially lower than at promoter regions (**Figure 2—figure supplement 1G**).

To further probe links between eRNA containing regions and enhancer activity, we partitioned the genome into a series of states via a Hidden Markov Model (HMM states) (**Figure 2—figure supplement 1H**). Positional information was used to mark these HMM states as promoter proximal or distal (**Figure 2—figure supplement 1I**). Re-evaluation of the eRNA expressing regions showed that 33% were associated with regions designated as enhancers (**Figure 2D**; compared to 4% genome-wide), with very few regions designated as quiescent or repressed (17% compared to 69% in randomly selected chromatin regions; **Figure 2—figure supplement 1J**).

The co-association of eRNA expressing regions with genomic elements associated with active chromatin marks is strongly suggestive of enhancer-like activity. However, to provide further evidence for active ongoing transcription at these loci we performed KAS-seq (**Wu et al., 2020**) in OE19 cells to identify areas of DNA strand opening as observed in the transcription bubble. The three replicates showed good congruency (**Figure 2—figure supplement 2A**), and we merged all three to call peaks of DNA strand opening (**Supplementary file 4**). These peaks show a highly significant overlap with the eRNA regions we identified from patient samples (**Figure 2—figure supplement 2B**), and higher levels of KAS-seq signal are associated with eRNA regions compared to random regions (**Figure 2E**). This is exemplified by eRNAs associated with a putative enhancer region located upstream from *JUP* (**Figure 2F**), *CCNE1* and *MYBL2* gene loci (**Figure 2—figure supplement 2C, D**). Furthermore, when we combined eRNA regions with regions showing KAS-seq peaks, higher levels of H3K27ac were observed compared to those lacking concomitant KAS-seq signal (**Figure 2—figure supplement 2E**), indicative of higher activity.

Finally, we focussed on potential super enhancers as these have been shown to play important roles in cancer-specific gene regulation (**Hnisz et al., 2013**) including gastroesophageal cancers (**Ooi**

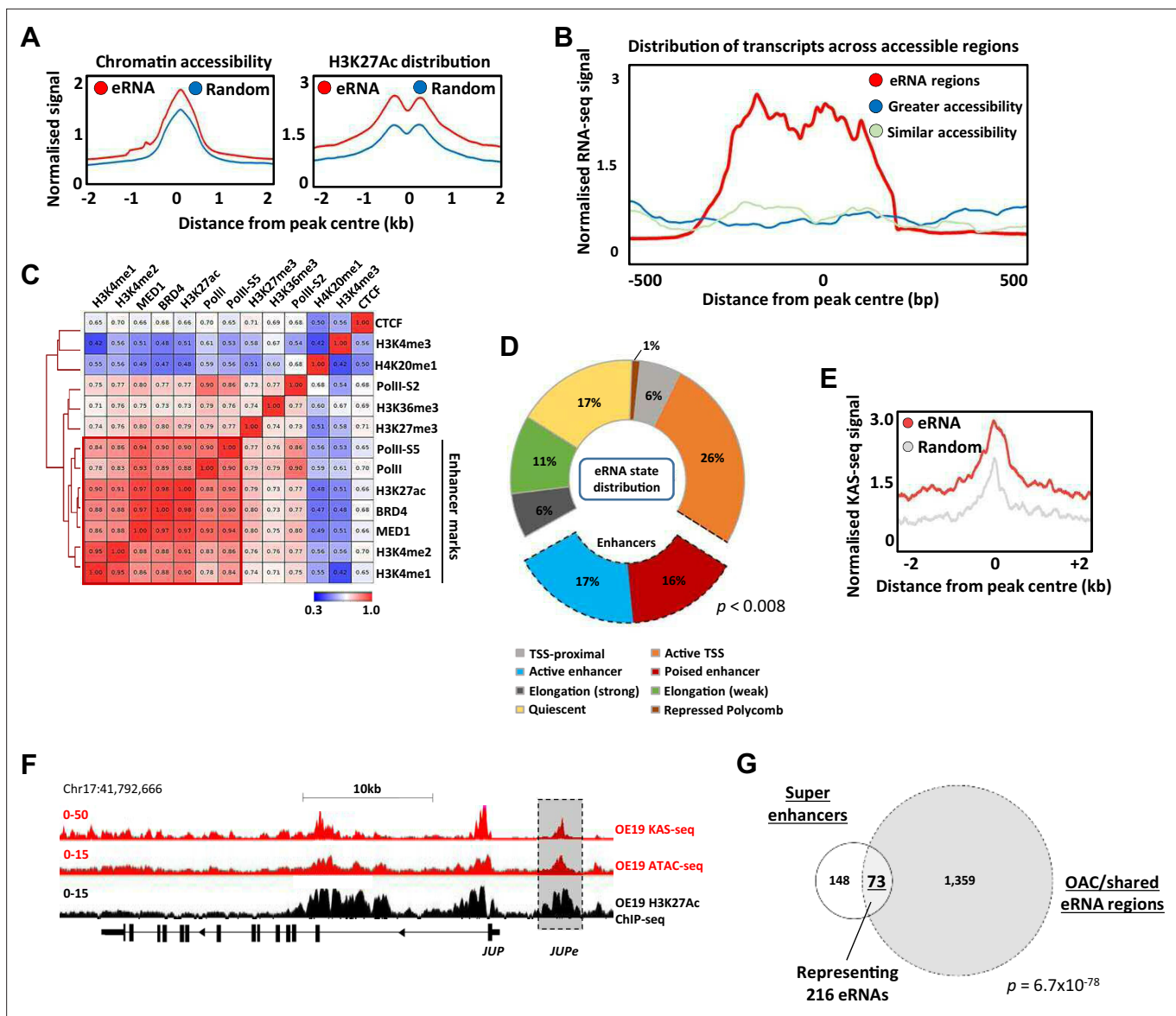


**Figure 2.** Putative enhancer RNAs (eRNAs) are associated with enhancer-like genomic regions. **(A)** Metplots of patient tissue chromatin accessibility (left) and OE19 cell H3K27ac ChIP-seq signal (right) at all 4600 eRNA regions compared to 4600 random regions of accessible chromatin. **(B)** Distribution of transcription at 4600 eRNA regions compared to 4600 randomly selected regions of similar or greater chromatin accessibility (regions shown as peak centre  $\pm 0.5$  kb). **(C)** Pearson's correlation and hierarchical clustering of CUT&Tag signal at 4600 eRNA regions for various chromatin-associated factors. **(D)** Distribution of ChromHMM emission states for 4600 eRNA regions. **(E)** Metplots of KAS-seq signal in OE19 cells at 4600 eRNA regions compared to 4600 random regions of accessible chromatin. **(F)** Genome browser view of OE19 KAS-seq, OE19 ATAC-seq data, and OE19 H3K27ac ChIP-seq at the *JUP* locus with the *JUPe* eRNA highlighted. **(G)** Venn diagram of overlap between 221 high-confidence intergenic super enhancers and 1432 eRNAs (specific to oesophageal adenocarcinoma [OAC] or shared with Barrett's oesophagus [BO] eRNA; p-value is shown; hypergeometric test). See also **Figure 2—figure supplements 1–3**.

The online version of this article includes the following figure supplement(s) for figure 2:

**Figure supplement 1.** Putative enhancer RNAs (eRNAs) are associated with enhancer-like genomic regions.

**Figure supplement 2.** KAS-seq reveals active transcription at enhancer RNA (eRNA) regions.

**Figure supplement 3.** Enhancer RNAs (eRNAs) are associated with super enhancers.

*et al., 2016*). We identified potential super enhancers in OE19 cells using HOMER (*Heinz et al., 2010; Whyte et al., 2013*) from peak sets generated from H3K27ac ChIP-seq (for histone activation marks) and ATAC-seq (for open chromatin) (**Figure 2—figure supplement 3A; Supplementary file 5**). We then overlapped these peak sets to generate a dataset with both indicators of super enhancer activity,

excluding promoter regions from our analysis. This resulted in 221 high-confidence super enhancers (**Figure 2—figure supplement 3B**). Next, the constituent enhancers within these super enhancers were overlapped with the eRNA regions we identified from OAC patients, producing a final list of 73 super enhancers showing evidence of eRNA activity, with a total of 216 eRNA regions residing in these super enhancers (**Figure 2G**). Multiple eRNA regions identified in patient samples are therefore associated with super enhancers as exemplified by the *ELF3* super enhancer (**Figure 2—figure supplement 3C**). The genes associated with these super enhancers are enriched in several biological processes with direct relevance to OAC, such as MAPK signalling and cadherin binding (**Figure 2—figure supplement 3D**).

Collectively, these data strongly indicate that the eRNA-associated regions we discovered in patient samples represent areas of enhancer activity due to the presence of enhanced accessibility, enhancer-associated chromatin marks/proteins, and evidence for actively transcribing RNA polymerase in OAC cells.

## Association of eRNA regions to target genes and regulatory transcription factors

Next, we asked whether we could identify upstream transcription factors that might control eRNA levels and provide insights into the regulatory landscape of OAC. First, we identified binding motifs for transcription factors that are over-represented in OAC or Barrett's-specific eRNA producing regions. This revealed enrichment for transcription factors previously identified as relevant for OAC including AP1, KLF5, and HNF1 (**Britton et al., 2017; Rogerson et al., 2019; Rogerson et al., 2020; Chen et al., 2020**) as well as CTCF, a factor implicated in enhancer activity (**Ren et al., 2017; Figure 3A; Supplementary file 6A**). However, the frequency of motif occurrence differed between eRNA- and open chromatin-defined enhancers in OAC patients; HNF1 motifs were significantly more enriched in eRNA-defined enhancers whereas AP1 and KLF5 motifs were more enriched in enhancers defined by increased accessibility alone (**Figure 3B**). A similar set of transcription factor motifs were observed when we omitted regions commonly found in patient samples and OE19 cells and instead focussed on eRNA-defined enhancers inferred only from OAC patient-specific ATAC-seq data (**Figure 3—figure supplement 1A**). AP1 motifs were again identified in Barrett's-specific regions as well as a different set of motifs including p53-binding motifs (**Figure 3A; Supplementary file 6B**). Similarly, calculating differential binding scores revealed higher binding activity of AP1 and HNF1 in OAC-specific regions and conversely higher p53-binding activity in Barrett's-specific regions (**Figure 3C; Supplementary file 7**). Thus, eRNA-defined enhancers reveal the activity of disease stage-specific transcriptional regulators. To further explore this point, we sought evidence for enhancer occupancy by transcription factors in OAC cells and found substantially more binding signal of KLF5 derived from ChIP-seq in OE19 cells **Rogerson et al., 2020** for eRNA-defined regions with KLF5 motifs compared to regions lacking the motif, or control genomic regions (**Figure 3D**). Furthermore, evidence for KLF5-mediated regulation was obtained by the significant overlap between the genes associated with the same eRNA regions (ie containing KLF5 motifs) and those genes downregulated upon KLF5 depletion in OE19 cells (**Figure 3E; Figure 3—figure supplement 1B–D; Supplementary file 1**). We also examined the effect of AP1 inhibition by expressing a dominant-negative FOS derivative (dnFOS; **Olive et al., 1997**) in OE19 cells (**Ogden et al., 2023**) and compared the downregulated gene profile with the eRNA-associated genes containing AP1 motifs that we have identified. Again, we observed a significant overlap between the genes associated with eRNA regions containing AP1 motifs in OAC samples and those genes downregulated upon AP1 inhibition (**Figure 3F; Figure 3—figure supplement 1E–G; Supplementary file 1**). To provide functional links between transcription factor occupancy at enhancers, enhancer activation and target gene transcription, we focussed on KLF5. ChIP-seq data **Rogerson et al., 2020** demonstrate that KLF5 strongly binds to the *JUP* and *CCNE1* enhancers but low levels are observed at the *MYBL2* enhancer (**Figure 3G**). KLF5 depletion (**Figure 3—figure supplement 1H**) caused reduced expression of all three target genes (**Figure 3H**). However only *JUP* and *CCNE1* enhancer activities were diminished following KLF5 depletion (**Figure 3I**), consistent with the higher occupancy of KLF5 at these enhancers compared to *MYBL2*. *MYBL2* is likely regulated by KLF5 through other cis regulatory elements or by an indirect mechanism. Our data are therefore consistent with KLF5 regulating *JUP* and *CCNE1* expression through the enhancers we have identified. Thus, both motif discovery and functional dissection demonstrate that KLF5 and AP1 are likely major players in eRNA-defined enhancer activation in OAC patients.

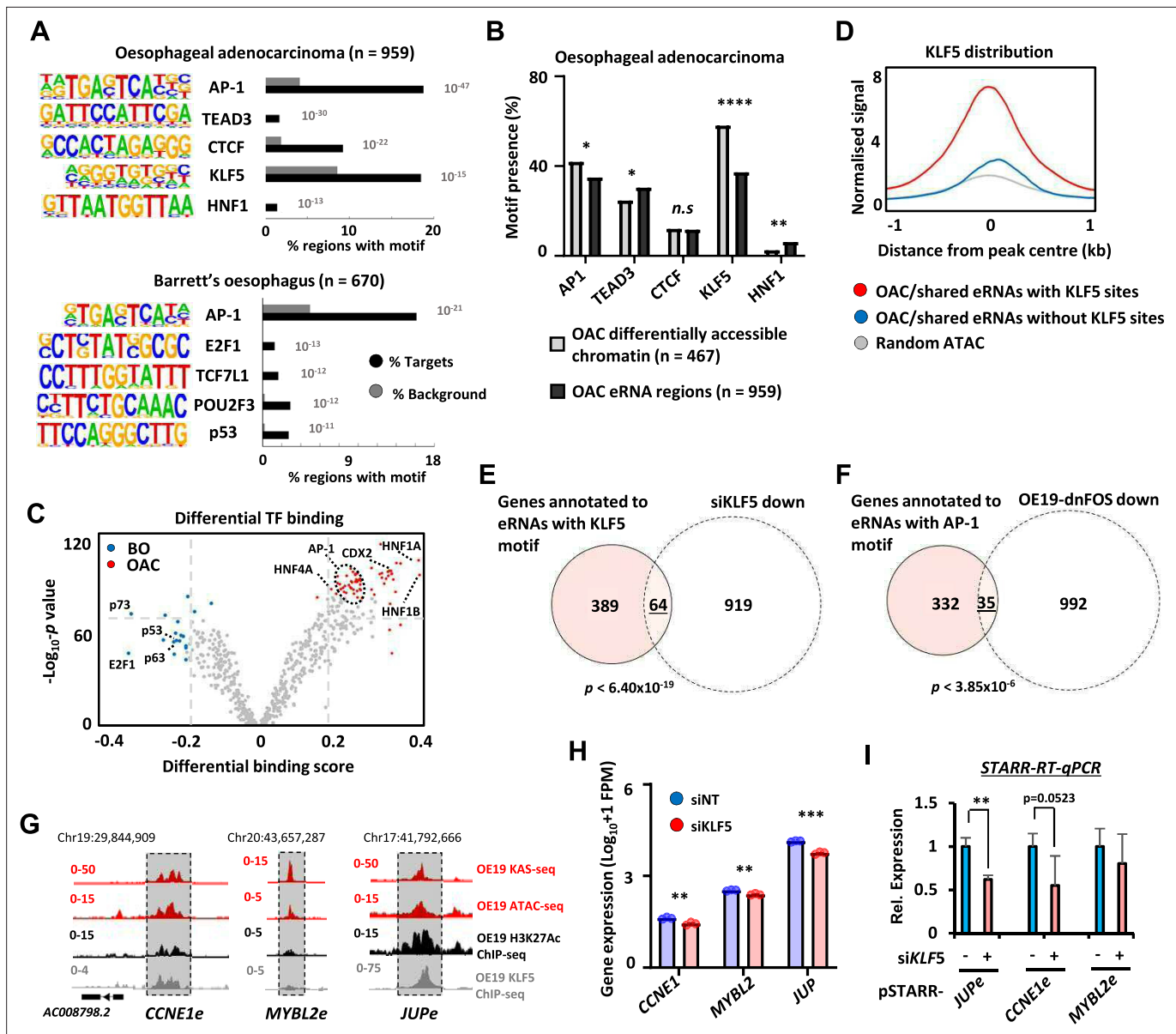


**Figure 3.** Association of enhancer RNA (eRNA) regions with transcriptional regulators. **(A)** Transcription factor de novo motif enrichment using HOMER, at eRNAs differentially expressed in oesophageal adenocarcinoma (OAC) (top;  $n = 959$ ) and Barrett's (bottom;  $n = 670$ ) ( $p$  values are shown). **(B)** Bar graphs displaying the frequency of motif prevalence of the top 5 enriched motifs at eRNA regions differentially expressed in OAC ( $n = 959$ ) compared to differentially accessible intergenic chromatin ( $****p < 0.0001$ ;  $**p < 0.01$ ;  $*p < 0.05$ ;  $N-1$  Chi-squared test). **(C)** Volcano plot showing differential TF binding ( $\pm 0.2$  differential binding score or  $\geq -\log_{10} P_{adj} 70$ ) at 4600 eRNAs regions using TOBIAS (Bentsen et al., 2020). **(D)** Metaplots of KLF5 ChIP-seq signal from OE19 cells at eRNAs (specific to OAC or shared with Barrett's oesophagus [BO] eRNA) containing a KLF5 motif, lacking a KLF5 motif or randomly selected open chromatin regions. **(E)** Venn diagram displaying overlap between genes annotated to KLF5 motif containing eRNAs (specific to OAC or shared with BO eRNA) with genes downregulated upon siKLF5 treatment ( $\text{Log}_2\text{FC} \geq 1.0$ ,  $p_{adj} = 0.05$ ) in OE19 cells ( $p$ -value is shown; Fisher's exact test). **(F)** Venn diagram displaying overlap between genes annotated to AP-1 motif containing eRNAs (specific to OAC or shared with BO eRNA) with genes downregulated upon dominant-negative FOS (dnFOS) induction ( $\text{Log}_2\text{FC} \geq 0.5$ ,  $p_{adj} = 0.05$ ) in OE19 cells ( $p$ -value is shown; Fisher's exact test). **(G)** Genome browser view of KAS-seq, ATAC-seq data, H3K27ac ChIP-seq, and KLF5 ChIP-seq in OE19 cells at the *CCNE1* (left), *MYBL2* (middle), and *JUP* (right) enhancer loci, with corresponding eRNA regions highlighted (5 kb window shown). **(H)** Bar graphs displaying the expression from RNA-seq analysis of *CCNE1*, *MYBL2*, and *JUP* genes in OE19 cells treated with siRNA targeting KLF5 ( $n = 3$ ;  $***p < 0.001$ ;  $**p < 0.01$ ; Welch's  $t$ -test). **(I)** Reverse-transcription quantitative real-time PCR (RT-qPCR) analysis of enhancer activity from the indicated pSTARR-enhancer vectors upon siKLF5 depletion in OE19 cells ( $n = 3$ ;  $**p < 0.01$ ;  $t$ -test). See also **Figure 3—figure supplement 1**.

The online version of this article includes the following figure supplement(s) for figure 3:

**Figure supplement 1.** Association of enhancer RNA (eRNA) regions with potential regulatory transcription factors.

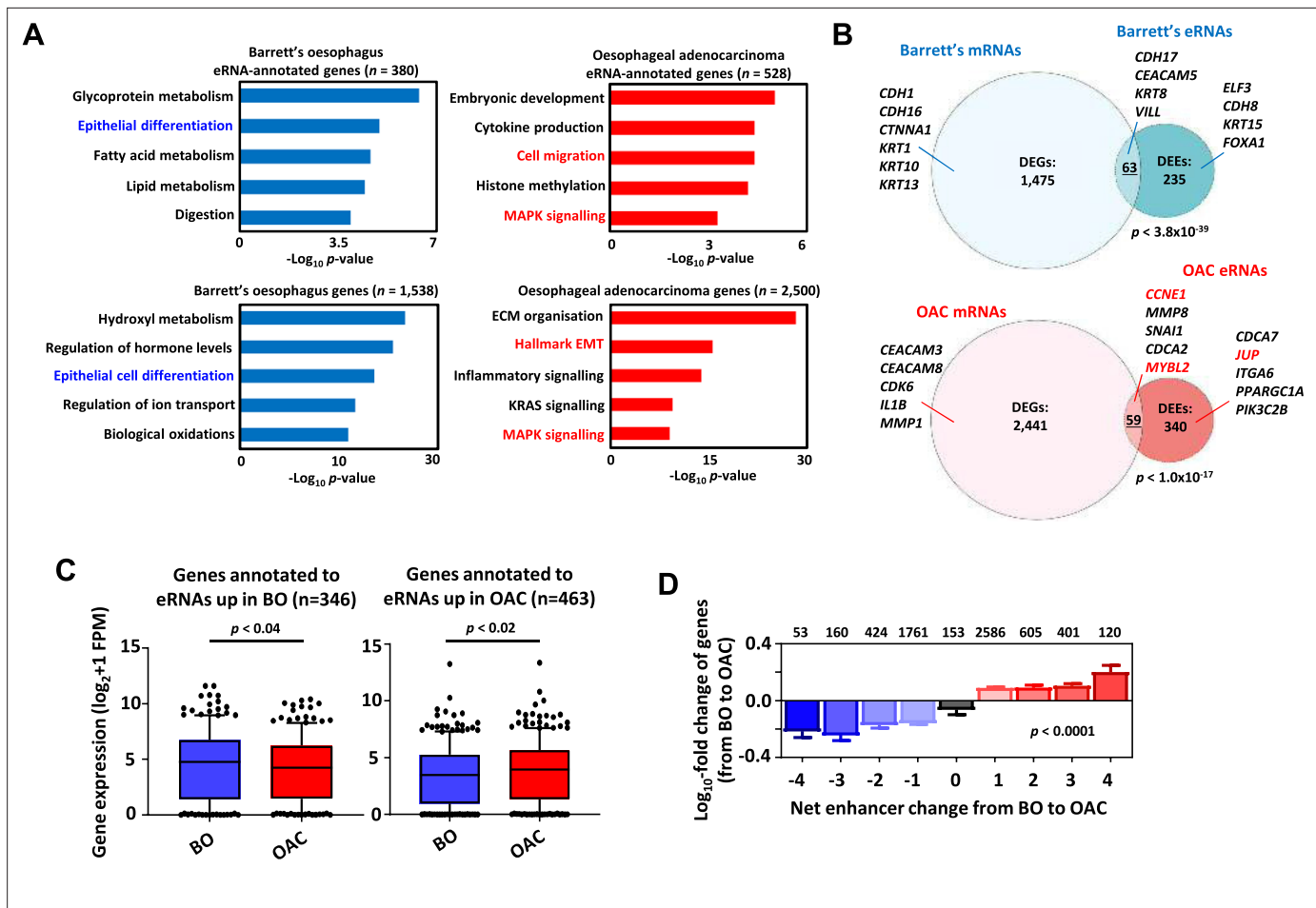


**Figure 4.** Association of enhancer RNA (eRNA) regions with transcriptional regulators and potential target genes. **(A)** Gene ontology (GO)-term analysis of differentially expressed eRNA region-associated genes (top-left/right) and differentially expressed genes (bottom-left/right) in Barrett's (left) ( $> \text{Log}_2\text{FC } 0.9$ ,  $< p_{\text{adj}} = 0.05$ ) and oesophageal adenocarcinoma (OAC, right) ( $> \text{Log}_2\text{FC } 1.1$ ,  $< p_{\text{adj}} = 0.05$ ). eRNAs were annotated to genes by the nearest gene model using HOMER (Heinz et al., 2010). **(B)** Venn diagram displaying overlap between differentially expressed genes and unique protein-coding genes annotated to differentially expressed eRNAs in Barrett's oesophagus (BO, top) and OAC (bottom) ( $p$ -value is shown; Fisher's exact test). **(C)** Box plots comparing the expression of genes annotated to eRNAs differentially expressed in BO (left) or OAC (right) in BO and OAC patient tissue total RNA-seq samples from the OCCAMS dataset ( $p$ -value is shown; Welch's  $t$ -test). **(D)** Genome-wide analysis of the effect of changing eRNA expression on gene expression within 200 kb chromosomal bins. Numbers above bars represent total genes associated with respective net-enhancer change ( $p$ -value is shown; Kruskal–Wallis test). See also **Figure 4—figure supplement 1**.

The online version of this article includes the following figure supplement(s) for figure 4:

**Figure supplement 1.** Association of enhancer RNA (eRNA) regions with potential target genes.

To understand the potential biological consequences of eRNA activation, we then linked the differentially active eRNA regions to putative target genes with the nearest gene model using HOMER (Heinz et al., 2010) resulting in 528 genes in OAC and 380 genes in Barrett's. Gene ontology (GO) analysis identified several terms relevant to the OAC phenotype such as 'Cell migration' and 'MAPK signalling' whereas Barrett's-specific regions identified genes associated with various metabolic processes and 'epithelial differentiation' that would be expected for this intestinal metaplastic tissue (Figure 4A). A similar set of GO terms were identified when we omitted regions commonly found in patient samples and OE19 cells and instead focussed on eRNA-defined enhancers inferred only from OAC patient-specific ATAC-seq data (Figure 3—figure supplement 1; Supplementary file 2). One difference was 'cell adhesion' which was more enriched in the patient-specific dataset which might reflect the differing adhesive properties on 2D cultured cells and cells growing in a 3D *in vivo* environment. We also performed differential gene expression analysis on the whole RNA-seq datasets to identify genes preferentially expressed in OAC or Barrett's and performed GO-term analysis (Supplementary file



**8, Supplementary file 9).** Similar GO terms were identified with ‘MAPK signalling’ and ‘Hallmark EMT/ECM organisation’ (terms associated with cell migration) resembling those identified through association with eRNA regions (**Figure 4A**). However, eRNA-associated genes revealed processes not among the top GO terms generated from differentially expressed genes (DEGs) such as ‘embryonic development’ and ‘histone methylation’. Similarly, Barrett’s-specific genes returned GO terms such as ‘epithelial cell differentiation’, as identified from eRNA regions further emphasising the similarity in biological processes identified by eRNA-associated genes and total RNAs. A range of different metabolic processes were also identified in both cases, illustrating the distinct information that is derived from eRNA-associated genes. To determine whether these similar GO categories reflected similar genes being identified, we overlapped the DEGs (**Supplementary file 8; Supplementary file 9**) with genes associated with differentially expressed eRNAs (DEEs **Supplementary file 2; Supplementary file 3**), that are enriched in either Barrett’s or OAC samples. We found a significant overlap between these sets of genes although the majority of the genes were uniquely identified by investigating either by total RNA-seq or by eRNA profiling (**Figure 4**). Therefore, despite pinpointing many similar biological processes, eRNA profiling reveals different candidate genes involved these processes.

To further investigate whether the activities of enhancer regions are linked to nearby gene expression, we selected eRNA regions preferentially expressed in either OAC or Barrett’s and found that the nearest genes exhibited higher expression in the correct corresponding tissue type in two independent datasets (**Figure 4C; Figure 4—figure supplement 1A**). This observation was further supported by comparing the expression of the genes closest to eRNA regions found in patient RNA-seq data to the expression of a random set of genes. This revealed significantly enhanced expression levels of eRNA-annotated genes in patients (**Figure 4—figure supplement 1B**). While the nearest gene model often correctly associates enhancers with the closest gene, this is not always the case, so we considered all genes within a 200 kb bin around the eRNA region rather than just the nearest gene. We then determined the net eRNA expression change when comparing Barrett’s to OAC samples and created nine bins reflecting the magnitude of differential expression. We then calculated the associated gene expression changes within these genomic bins when comparing Barrett’s to OAC. There was a clear correlation between the directionality of eRNA expression with mRNA expression which changed in an analogous manner, with high eRNA levels in OAC associated with higher gene expression in OAC and vice versa in Barrett’s (**Figure 4D**).

In summary therefore, eRNA expression profiling can reveal specific upstream regulatory transcription factors and the eRNA generating regions can be used to uncover a set of biological processes and constituent genes that are relevant to specific disease states.

## Target genes of eRNA-defined enhancers are co-expressed in OAC

We identified potential target genes of eRNA-defined enhancers by implementing the nearest gene model (**Figure 4B**). However, the nearest gene is not always the enhancer target (**Sanyal et al., 2012**). We therefore examined the correlation between eRNA expression and the expression of their designated target genes for three candidate enhancers, localised in the vicinity of the *JUP* (**Figure 5A**), *MYBL2*, and *CCNE1* (**Figure 5—figure supplement 1A, B**) loci. Each of these putative enhancer regions contains more RNA signal in OAC compared to Barrett’s as well as evidence for chromatin accessibility in OAC patient material. We focussed on *JUP* as this had not been implicated in OAC previously and is significantly co-amplified with *ERBB2*, a key oncogenic driver of OAC (**Cancer Genome Atlas Research Network et al., 2017; Frankell et al., 2019; Figure 5—figure supplement 1C**). Indeed, both *JUP* transcript and eRNA are upregulated compared to Barrett’s in OAC patients with high *ERBB2* expression (**Figure 5B**). We performed a similar analysis for *CCNE1* and *MYBL2* but instead examined their expression across all OAC samples. For both loci, the eRNA and gene transcript are both upregulated in OAC relative to Barrett’s (**Figure 5—figure supplement 1D, E, )**. Next, we examined the correlation of eRNA and transcript expression on a ‘sample by sample’ basis. *JUP* eRNA expression showed strong correlation with *JUP* expression, irrespective of *ERBB2* level sample status (**Figure 5C**). Lower correlations were observed with the expression of the two adjacent genes (**Figure 5—figure supplement 1F**) consistent with *JUP* being the relevant target. The correlation between *JUP* eRNA and *JUP*-coding gene expression was even higher when only OAC samples are compared, and this correlation is much lower in Barrett’s samples (**Figure 5—figure supplement 1G**). Similarly, *CCNE1* and *MYBL2* eRNA expression is more strongly correlated with the expression of their

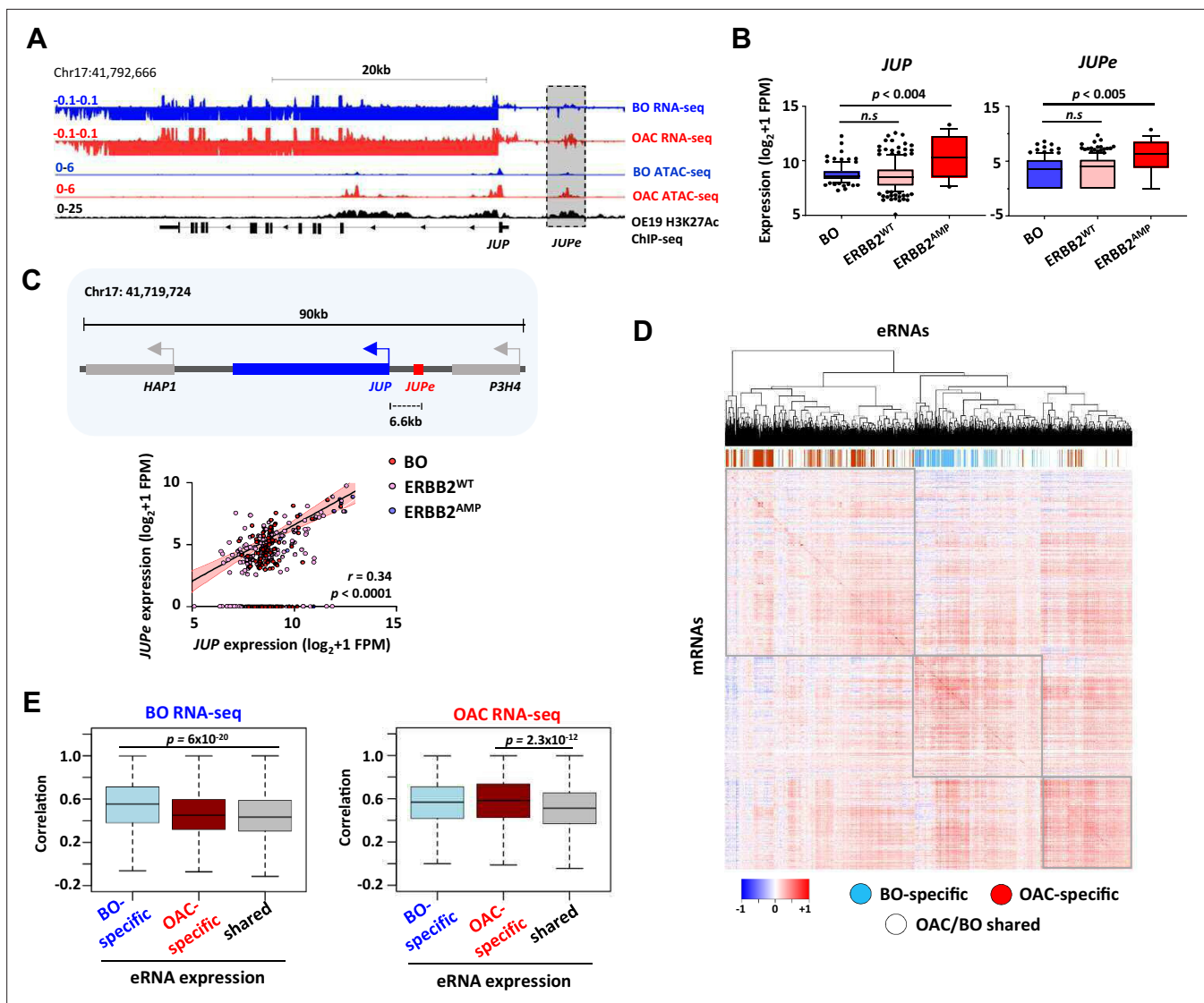


**Figure 5.** Enhancer RNA (eRNA) regions identify *JUP* as a candidate target gene. **(A)** Genome browser view of Barrett’s oesophagus (BO) and oesophageal adenocarcinoma (OAC) patient tissue ATAC- and total RNA-seq data, and H3K27ac ChIP-seq in OE19 cells, at the *JUP* locus with the *JUPe* eRNA highlighted. **(B)** Box plots comparing the expression of *JUP* (left) and *JUPe* (right) in BO ( $n = 108$ ), ERBB2<sup>WT</sup> ( $n = 193$ ), and ERBB2<sup>AMP</sup> ( $n = 17$ ) OAC patient tissue total RNA-seq samples ( $p$ -value is shown; Welch’s  $t$ -test). **(C)** Schematic displaying relative locations of putative eRNA region target genes and nearest neighbours (top) and correlation of *JUPe* with *JUP* expression across BO ( $n = 108$ ), ERBB2<sup>WT</sup> ( $n = 193$ ), and ERBB2<sup>AMP</sup> ( $n = 17$ ) OAC patient tissue total RNA-seq samples (bottom) (Spearman’s  $r$  and  $p$ -value are shown; Spearman’s rank correlation test). **(D, E)** Global analysis of correlations of eRNA expression with the expression of the most correlated gene within a 200 kb window flanking the eRNA region. eRNAs are defined as tissue-specific according to **Figure 1A**, and the rest of the eRNAs are designated as shared. **(D)** Heatmap showing the correlation coefficients between all 4600 eRNAs and the most highly associated mRNAs in the RNA-seq datasets. Samples are clustered based on these correlation coefficients. OAC-specific eRNAs (red), BO-specific eRNAs (blue), and shared eRNAs (white) are indicated across the top. **(E)** Box plots showing the correlations with BO gene expression datasets (left) or OAC gene expression datasets (right). Significance values ( $t$ -test) are shown between the indicated groups. See also **Figure 5—figure supplement 1**.

The online version of this article includes the following figure supplement(s) for figure 5:

**Figure supplement 1.** Enhancer RNA (eRNA) regions identify *JUP*, *CCNE1*, and *MYBL2* as a candidate target genes.

designated targets than either of their immediately flanking genes (**Figure 5—figure supplement 1H, I, J**). We extended this analysis across all eRNAs and asked whether we could find significantly correlated mRNA expression of genes located in their vicinity ( $\pm 100$  kb)(**Supplementary file 10**). Generally, highly correlated genes could be identified (see diagonal in **Figure 5D**). Interestingly when we clustered the data according to the expression of the genes associated with each eRNA, then

there was generally a good segregation of OAC- and BO-specific eRNAs further emphasising the relevance of the correlations we observed (**Figure 5D**). Furthermore, when we split the RNA-seq data into tissue types, there was a significantly higher correlation of BO-specific eRNA with nearby gene expression in BO datasets, compared to analysing the shared eRNAs (**Figure 5E**, left). Similarly, the same trend was observed for OAC-specific eRNAs which were more highly correlated with nearby gene expression in OAC datasets (**Figure 5E**, right).

Together these results demonstrate that we are able to link eRNA expression to their putative targets in the relevant disease-specific datasets.

## Validation of enhancer activity of eRNA regions

To validate that the regions generating eRNAs have enhancer activity we again focussed on the *JUP*, *MYBL2*, and *CCNE1* loci. First, we showed that all three putative enhancer regions have significantly higher levels of KAS-seq signal in OE19 cells relative to a control enhancer from the *APOL4* gene that is not expressed in OE19 cells (**Figure 6A**). This is reflective of ongoing transcription. Furthermore, all three eRNAs and their associated target genes exhibit higher expression in OE19 cells compared to the Barrett's CP-A cell line (**Figure 6B**). To directly establish enhancer activity, we cloned the regions encompassing the eRNAs into two different enhancer reporter systems with either RNA (**Figure 6C**) or luciferase (**Figure 6—figure supplement 1A**) readouts. For all three regions, both assays demonstrated significant enhancer activity in OE19 cells (**Figure 6C** and **Figure 6—figure supplement 1A**). Finally, we used an inducible dCas9-KRAB synthetic repressor protein to silence the activities of each enhancer in their natural chromatin context in OE19 cells (**Figure 6—figure supplement 1B**). In all cases, introduction of the relevant sgRNA to target the dCas9-KRAB repressor to the putative enhancer, resulted in reduced eRNA transcription and reduced expression of the associated target gene, albeit to a lesser degree in the case of the target genes (**Figure 6D**). The latter observation is not unexpected as a combination of several proximal and distal regulatory elements rather than a single enhancer likely contributes to their expression. Importantly, no significant changes in expression were observed for any of the genes immediately flanking the target genes, demonstrating the fidelity of our enhancer–gene linkages (**Figure 6—figure supplement 1C**). However, to establish whether any additional longer range enhancer–gene linkages could be found, we used Hi-C to generate a 3D chromatin map in OE19 cells. Replicate samples showed good reproducibility (stratum-adjusted correlation coefficient = 0.965). However, we were unable to identify any long range interactions emanating from the *CCNE1e* and *MYBL2e* enhancer regions (**Figure 6—figure supplement 2A, B**). In contrast, we identified significant long range linkages between the *JUPe* enhancer and the region located downstream from the *ERBB2* locus (**Figure 6E**). This juxtapositioning likely arises due to genomic rearrangements that are seen in OAC where *JUP* is often located on the same ecDNA amplicons as *ERBB2* (**Ng et al., 2022**). We tested whether any of the genes in the vicinity of the contact point are also regulated by the *JUPe* region and found that *GRB7* expression is reduced upon reducing *JUPe* activity, but no effect is seen on *ERBB2* or *MIEN1* expression (**Figure 6F**). *GRB7* expression is also reduced following *KLF5* depletion, consistent with the role of *KLF5* in activating this enhancer region (**Figure 6—figure supplement 2C**).

Together these results build on our correlative observations linking eRNA containing regions with enhancer-like properties and provide definitive proof of enhancer activity and regulatory linkage to neighbouring genes.

## Biological and clinical relevance of eRNAs and their target genes

We have shown that the discovery of eRNAs in OAC patients reveals genes and processes which are operative in OAC and allows us to distinguish OAC from Barrett's patients. To provide further biological insights, we asked whether any of the three eRNA target genes, *JUP*, *MYBL2*, and *CCNE1* were uncovered in a cell line viability screen in the DepMap project (**Tsherniak et al., 2017; Behan et al., 2019**). We found that four of the top 6 cell lines showing a dependency on *JUP* expression are gastroesophageal in origin and these all contain *ERBB2* amplifications (**Figure 7A**, left). *JUP* is also the highest scoring gene for fitness dependency across OAC cell lines (**Figure 7A**, right). In contrast, *GRB7* which is also *JUPe*-regulated does not majorly contribute to the fitness of OAC cell lines (**Figure 7—figure supplement 1A**). Similarly, *MYBL2* and *CCNE1* did not score highly in this screen. We therefore further probed the function of the eRNA-defined enhancers in the OE19 OAC cell line

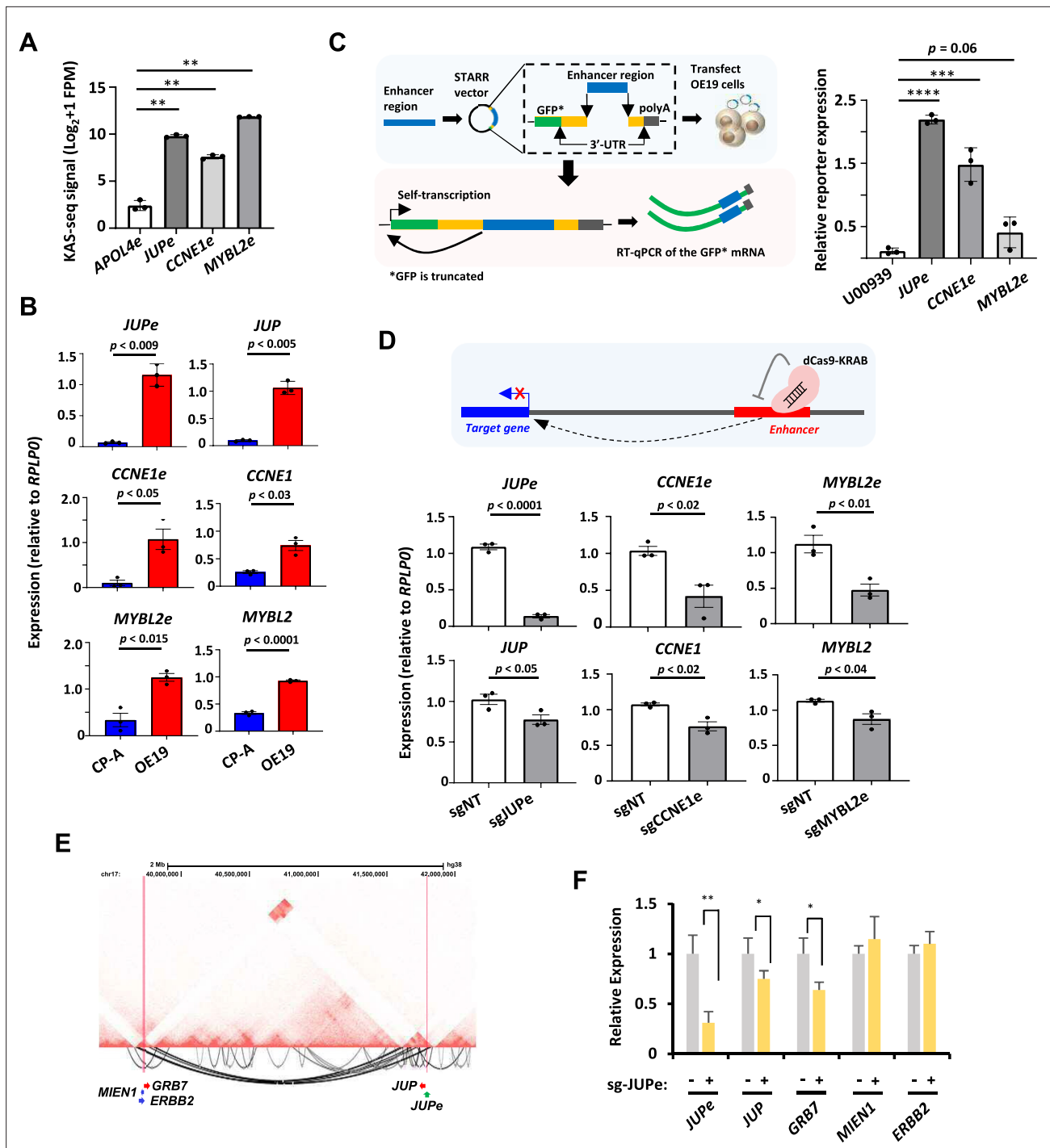


**Figure 6.** In vitro interrogation of enhancer RNA (eRNA) regions confirms production and association with cancer-associated processes. **(A)** Bar graphs displaying KAS-seq signal at the *APOL4e*, *JUPe*, *CCNE1e*, and *MYBL2e* regions in OE19 cells ( $n = 3$ ;  $**p < 0.01$ ; Welch's  $t$ -test). **(B)** Bar graphs displaying difference in expression of *JUP*, *CCNE1*, *MYBL2* and *JUPe*, *CCNE1e*, and *MYBL2e* between CP-A and OE19 cells using RT-qPCR ( $n = 3$ ; p-value is shown; Welch's  $t$ -test; \*GFP is truncated). **(C)** Schematic of STARR-RT-qPCR assay (left) and bar graph displaying the difference in STARR reporter activity between *JUPe*, *CCNE1e*, and *MYBL2e*, compared to U00930 tRNA-negative eRNA control (right) ( $n = 3$ ;  $****p < 0.0001$ ;  $***p < 0.001$ ; one-way analysis of variance (ANOVA) with Bonferroni's correction). **(D)** Bar graphs displaying the expression of *JUPe*, *CCNE1e*, and *MYBL2e* eRNAs (top) and *JUP*, *CCNE1*, and *MYBL2* mRNAs (bottom) in OE19-dCas9-KRAB cells using real time RT-qPCR, upon treatment with the indicated targeting or non-targeting (NT) sgRNA ( $n = 3$ ; p-value is shown; Welch's  $t$ -test). A schematic of dCas9-KRAB targeting of eRNA regions is shown. **(E)** Genome browser view of Hi-C data surrounding the *JUP* locus. Significant intrachromosomal interactions are shown below the tracks. The start (at *JUPe*) and end (near *ERBB2*) of long-range interactions are indicated.

Figure 6 continued on next page

Figure 6 continued

range loops are highlighted with red lines. (F) RT-qPCR analysis of expression of the indicated genes or *JUP* eRNAs following dKAS9-KRAB-mediated repression of *JUP* activity ( $n = 3$ ; \*\* $p < 0.01$ , \* $p < 0.05$ ; Welch's t-test). See also **Figure 6—figure supplements 1 and 2**.

The online version of this article includes the following source data and figure supplement(s) for figure 6:

**Figure supplement 1.** In vitro interrogation of enhancer RNA (eRNA) regions confirms production and association with cancer-associated processes.

**Figure supplement 1—source data 1.** Raw unedited images of Western blots.

**Figure supplement 1—source data 2.** Original TIFF files used to create Figure 8, **Figure 6—figure supplement 1b**.

**Figure supplement 2.** HiC analysis of OE19 cells.

by using the dCas9-KRAB silencing system directed at these regions. In all cases, enhancer silencing led to significant reductions in cell viability and growth (**Figure 7B**; **Figure 7—figure supplement 1B**).

To provide further clinical relevance, we used an RNA-seq dataset from the TCGA consortium (**Cancer Genome Atlas Research Network et al., 2017**) that differed from our discovery cohort to ask whether any of the eRNA target genes informed on any particular clinical features. We found that the age of diagnosis was lower in patients expressing high levels of *MYBL2* (**Figure 7C**) and *JUP* (**Figure 7—figure supplement 1C**) suggesting earlier disease onset. Furthermore, in the case of *MYBL2*, high-level expression was indicative of lower median survival times (**Figure 7D**), although *JUP* and *CCNE1* were not informative in that regard (**Figure 7—figure supplement 1D**). For *JUP*, this is not unexpected as it is only amplified in a subset of patients where co-amplification with *ERBB2* is often observed (**Figure 7—figure supplement 1C**). Altogether, 32% of genes annotated to OAC-specific eRNAs displayed a significant prognostic value for patient survival (**Figure 7—figure supplement 1E**). Finally, we took an unbiased approach and asked whether we could identify a clinically

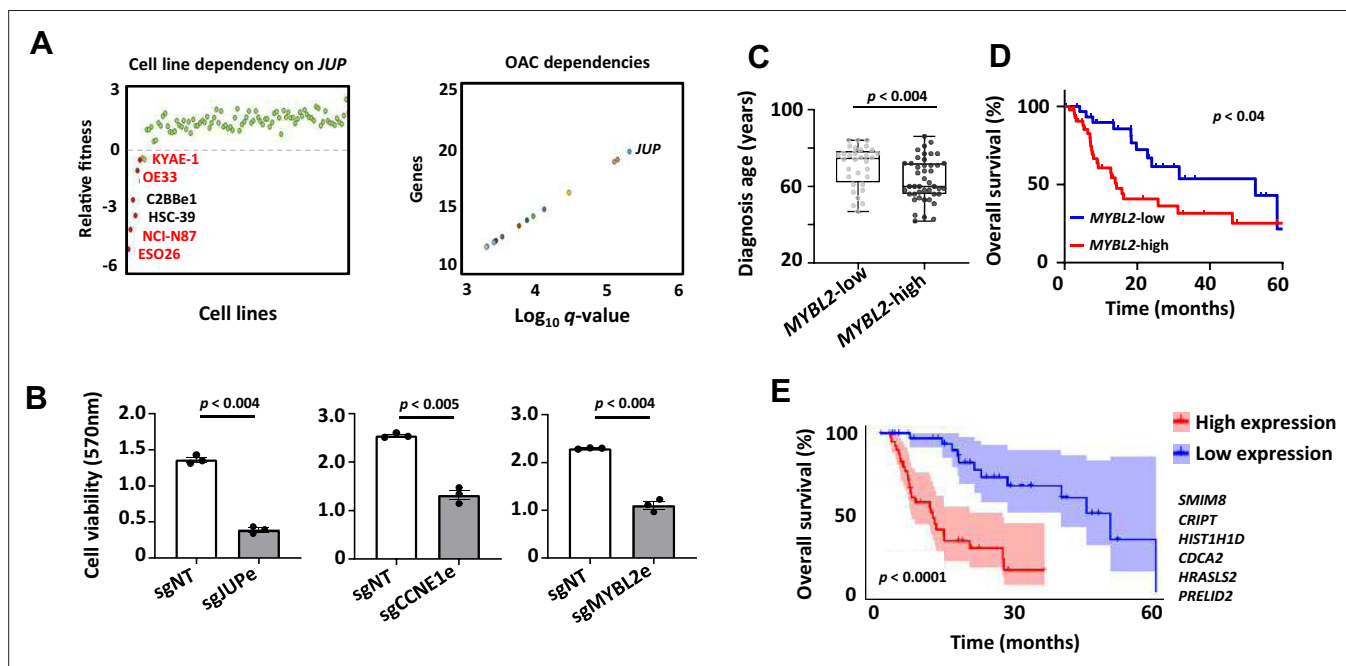


**Figure 7.** Biological and clinical relevance of enhancer RNAs (eRNAs) and their target genes. (A) Scatter plots displaying data from the Sanger DepMap Project Score (Tsherniak et al., 2017; Behan et al., 2019) highlighting cell line dependency on *JUP* (left) (gastroesophageal cell lines are marked in red) and top genetic dependencies in oesophageal adenocarcinoma (OAC, right). (B) Bar graph displaying the difference in cell viability in OE19-dCas9-KRAB cells upon sgRNA treatment, assessed by crystal violet assay ( $n = 3$ ; p-value is shown; Welch's t-test). (C) Box plots comparing diagnosis age for OAC patients with low and high *MYBL2* expression in the TCGA PanCancer Atlas dataset (p-value is shown; Welch's t-test). (D) Kaplan-Meier plot comparing overall survival between OAC patients with low and high *MYBL2* expression in the TCGA PanCancer Atlas dataset (Log rank p-value is shown). (E) Kaplan-Meier plot comparing overall survival between OAC patients with low and high signature eRNA target expression in the TCGA PanCancer Atlas dataset (Log rank p-value is shown; signature genes are shown). See also **Figure 7—figure supplement 1**.

The online version of this article includes the following figure supplement(s) for figure 7:

**Figure supplement 1.** Biological and clinical relevance of enhancer RNAs (eRNAs) and their target genes.

significant signature within the entire eRNA-associated gene list. This revealed a six-gene signature that was highly predictive of OAC patient survival (**Figure 7E**). Only three out of six genes comprising this signature were annotated to OAC DEEs. We therefore also explored whether we could derive a prognostic signature from OAC unique DEE-annotated genes, OAC unique DEGs or the intersect of OAC DEEs and DEGs (as defined in **Figure 4B**) and identified differing prognostic signatures in all categories (**Figure 7—figure supplement 1F**). DEEs are therefore able to predict prognostic signatures on their own to an equivalent level as using DEGs but do so by providing alternative molecular markers to assess patient prognosis.

Collectively, these data demonstrate the functional importance of the eRNA-defined enhancers and their target genes for OAC cell growth and their potential utility for assessing patient prognosis. In the case of *JUP*, the broad OAC cell dependency suggests that this represents a target of potential therapeutic value, especially in *ERBB2*-positive patients.

## Discussion

Cancer is driven by a combination of genetic and epigenetic changes (reviewed in **Zhao et al., 2021**). Both of these processes ultimately lead to alterations in the activity of gene regulatory elements, including transcriptional enhancers, that results in a change in cellular phenotype that defines the tumourigenic state. While profiling of histone marks and chromatin accessibility is useful in defining potential gene regulatory elements, this approach is limited for defining active enhancers. Here, we used eRNA profiling to identify regions harbouring potentially active enhancers in OAC patient samples. We integrated these with a range of epigenetic datasets and experimentally validated several regions as *bona fide* enhancers. Importantly, our enhancer repertoire identified new molecular events that are activated in OAC which were not apparent from either genome sequencing or mRNA profiling alone.

A previous pan-cancer analysis of RNA-seq datasets generated by the TCGA consortium to identify eRNAs defined a compendium of potential enhancers across human cancers and demonstrated how they could have clinical significance (**Chen et al., 2018**). However, while the authors examined oesophageal cancers, they mixed two distinct disease sub-types, squamous and adenocarcinoma, which limited any discoveries specific to OAC. Here, we specifically interrogated OAC RNA-seq data (generated by the OCCAMs consortium) and to identify enhancers that are potentially relevant to OAC, we compared their associated eRNA levels to the pre-cancerous BO state. Using this approach, we were able to identify ~1000 high-confidence OAC-specific enhancers. These enhancer regions exhibited high accessibility in both patient samples and cell line models and using a variety of chromatin marks profiled in an OAC cell line model we provided further verification of the enhancer-like properties. The OAC-specific enhancers are associated with transcription factors which have been shown to be important for driving OAC-specific transcriptional events (e.g., KLF5, **Rogerson et al., 2020**; AP1, **Britton et al., 2017**). Reciprocally we also identify ~700 Barrett's-specific enhancers which are associated with a different transcription factor repertoire, including the potential involvement of members of the TP53/TP63/TP73 family. While we have identified a large number of intergenic enhancers, the approach we have taken will miss intragenic enhancers, and other approaches using function-based assays (e.g., STARR-seq; **Arnold et al., 2013**) or computational imputation will be needed to identify these.

Our newly derived eRNA-defined enhancer datasets also provide novel insights into pathways that are operational in OAC. This is apparent from the limited overlap in DEGs at the mRNA level versus the differential expression of genes associated with nearby enhancers defined by eRNA levels. Interestingly while the specific gene overlaps are limited, the broad processes defined by GO terms such as MAPK signalling and cell migration/EMT remain the same. Part of this discrepancy might be explained by the OAC-specific enhancers maintaining gene expression in the BO–OAC transition rather than de novo gene activation in OAC or alternatively that many genes may be primarily driven by changes in promoter rather than enhancer activity. However, expression change cut offs we use may also contribute to this, as can the heterogeneity of the OAC samples. Other potential reasons for the lack of congruency include technical issues such as the nearest gene model may not always provide the most appropriate linkage of eRNAs to target genes and that we are likely missing many eRNAs due to the datasets we used which are not optimally designed for eRNA identification. An enhancer associated with *JUP* was specifically revealed by eRNA profiling, alongside hundreds of

other enhancers linked to genes involved in oncogenic processes such as cell migration, PI3K signaling, and metabolism. We validated this *JUP* enhancer, and enhancers linked to *MYBL2* and *CCNE1*, and their association with their proposed targets by CRISPRi. Furthermore, correlations between eRNA and mRNA expression across cancer samples suggest a causal link. Longer range regulatory interactions were detected between the *JUP* enhancer and *GRB7*, but HiC analysis did not reveal any additional potential connections for the other two enhancers. It remains possible that such long regulatory interactions may exist that escaped detection using HiC. Importantly both *CCNE1* and *MYBL2* play important roles in promoting cell proliferation, an important cancer cell trait. *JUP* (otherwise known as junction plakoglobin) had not previously been implicated in OAC but this was identified in a screen for gene dependencies in OAC cell lines (DepMap project: *Tsherniak et al., 2017; Behan et al., 2019*) and we validated its importance for OAC cell growth. In this context, the co-amplification with *ERBB2* is intriguing as both genes are on the same chromosome and are ~2 Mb apart and the intervening region is not usually co-amplified. Both can be found on the same ecDNA molecules (*Ng et al., 2022*) allowing closer juxtapositioning of *ERBB2* and the *JUPe* enhancer, which we were able to validate using HiC in OE19 cells. Nevertheless, we were unable to detect *JUPe* enhancer-mediated *ERBB2* regulation. This co-amplification may instead reflect a functional interdependency for these two oncogenic events. *JUP* has previously been implicated in multiple cancers although it is generally found to be a tumour suppressor protein, rather than the oncogenic properties it has in the context of OAC (reviewed in *Aktary et al., 2017*). As *JUP* encodes a protein involved in cell–cell contacts, this might suggest a role for this process in OAC cancer cell survival and a potential route to therapy. Alternatively, *JUP* may be acting via the numerous other cellular processes in which it has been implicated, and further work is needed to understand the precise role it has in OAC cells.

In addition to pointing to potential actionable pathways, we also demonstrate that eRNA profiling is clinically relevant and is sufficient to differentiate between BO and OAC. A six-gene signature derived from our OAC-specific enhancer-associated genes is able to predict prognostic outcomes. Indeed, a large proportion of the eRNA-associated genes show prognostic significance when analysed on an individual basis. Furthermore, by focussing in on a few examples, we found that one of the novel OAC-associated genes, *JUP*, was upregulated in *ERBB2* overexpressing OAC samples which is reflected by their frequent co-amplification. Coupled with the observation that *JUP* is required for the survival of a range of OAC cell lines harbouring *ERBB2* amplifications, this further emphasises the potential utility of *JUP* as a therapeutic target in this subset of OAC patients. This would provide an alternative approach to the use of *ERBB2* inhibitors which are routinely administered but have limited therapeutic benefit (*Bang et al., 2010*). Further clinical insights are provided by other eRNA-defined enhancer regions, such as the enhancer associated with *MYBL2* where high *MYBL2* expression indicates a worse prognosis for patients and earlier disease onset.

In summary, we identify a cohort of OAC-specific enhancers, expanding our knowledge of the regulatory networks that are operational in OAC. This has led to novel insights into the pathways that are operational in this disease. The approach we have taken to identify cancer-specific enhancers should be broadly applicable to other tumour types or subtypes, where data are available for both the cancer and the originating normal or pre-cancerous tissue.

## Materials and methods

### Cell culture and treatments

OE19 cells were purchased from ATCC and tested negative for mycoplasma. OE19 cells were cultured in RPMI 1640 (Thermo Fisher Scientific, 52400) supplemented with 10% foetal bovine serum (Thermo Fisher Scientific, 10270). OE19-dCas9-KRAB stable cells were previously generated from the parental OE19 cells (*Rogerson et al., 2020*) and cultured as above with the addition of 500 ng/ml puromycin (Sigma P7255). The expression of dCas9-KRAB was induced using 100 or 250 ng/ml doxycycline (Sigma-Aldrich, D3447). Cell lines were cultured at 37°C, 5% CO<sub>2</sub> in a humidified incubator.

### dnFOS over-expression

pINDUCER20-GFP-AFOS (ADS5006, *Britton et al., 2017*) was packaged into lentivirus and OE19 cells were transduced with lentivirus as previously described (*Tiscornia et al., 2006*). Briefly, 3 × 10<sup>6</sup> HEK293T cells were transfected with 2.25 µg psPAX2 (Addgene, 12260), 1.5 µg pMD2.G (Addgene,

12259), and 3  $\mu\text{g}$  pINDUCER20-GFP-AFOS using PolyFect (Qiagen, 301107). Media was collected at 48 and 72 hr post-transfection and viral particles were precipitated using PEG-it Solution (System Biosciences, LV810A-1). To transduce, cells were treated with virus (Multiplicity of Infection (MOI) 0.5–1.0) and 5  $\mu\text{g}/\text{ml}$  Polybrene (EMD Millipore, TR-1003). Polyclonal cells were selected for 2 weeks in 250  $\mu\text{g}/\text{ml}$  G418 (Thermo Fisher Scientific, 10131027). dnFOS (*Olive et al., 1997*) was induced with 1  $\mu\text{g}/\text{ml}$  doxycycline.

### sgRNA transfection

$2 \times 10^5$  cells were transfected with 10 pmol sgRNA pool using Lipofectamine RNAiMAX transfection reagent (Thermo Fisher Scientific, 13778150) according to the manufacturer's instructions. Cells were seeded into 6-well plates. Modified full-length sgRNAs were designed using E-CRISP (*Heigwer et al., 2014*) and off-target activity assessed using CCTop (*Stemmer et al., 2015*). sgRNAs were ordered from Synthego. sgRNA sequences are listed in *Supplementary file 11*.

### Cell growth and cell viability assays

Cell growth and viability were assessed by crystal violet assay. Assays were performed by fixing cells in 4% paraformaldehyde for 10 min. Cells were stained with 0.1% crystal violet (Sigma-Aldrich, HT90132) for 30 min. Crystal violet dye was extracted using 10% acetic acid and absorbance readings taken at 570 nm on a SPECTROstar Nano Microplate Reader (BMG LABTECH). Cell growth measurements were taken at 0, 24, 48, and 72 hr and cell viability measurements taken at 72 hr.

### RT-qPCR and eRNA qPCR

Total RNA was extracted from cells using an RNeasy Plus RNA extraction kit (Qiagen, 74136) according to the manufacturer's protocol. RT-qPCR reactions were run using the QuantiTect SYBR Green RT-qPCR kit (Qiagen, 204243) on a Qiagen Rotor-Gene Q. For eRNA-qPCR, RNA was extracted using an RNeasy Plus RNA extraction kit (Qiagen, 74136) with the on-column DNase digest, according to the manufacturer's instructions. 500 ng of RNA was reverse-transcribed using SuperScript VILO Master Mix (Thermo Fisher Scientific, 11755250) according to the manufacturer's instructions. eRNA levels were assessed by qPCR using a Rotor-Gene SYBR Green PCR Kit (Qiagen, 1054586) on a Qiagen Rotor-Gene Q. Relative transcript levels were determined by standard curve and normalised to the expression of *RPLP0* control gene. Primers used are listed in *Supplementary file 11*.

### Luciferase and STARR-qPCR reporter assays

Regions containing JUPe, MYBL2e, or CCNE1e were amplified from OE19 genomic DNA using primers containing 20 bp overlap regions with the multiple cloning site of the pGL3 Promoter vector (Promega, E1761) for luciferase assays, or between the InFusion arms of the hSTARR\_ORI vector (Addgene, 99296) (*Supplementary file 11*). Final vectors were assembled using HiFi assembly (NEB, E5520S) according to the manufacturer's instructions to create plasmids containing JUPe, MYBL2e, or CCNE1e enhancer regions in either hSTARR\_ORI (pAS5008-pAS5010) or pGL3- vectors (pAS5011-pAS5013). All recombinant plasmids are available upon request. Enhancer vectors were transfected using the Amaxa Nucleofector II (Lonza) with Cell Line Nucleofector™ Kit V (Lonza, VCA-1003) and program T-020, according to the manufacturer's instructions. For luciferase assays, 250 ng of enhancer vector was co-transfected alongside 50 ng of pCH110 (Amersham). For STARR-qPCR, 800 ng of vector was transfected. Enhancer activity was assessed using the Dual-Light Luciferase &  $\beta$ -Galactosidase Reporter System (Thermo Fisher Scientific, T1003) according to the manufacturer's instructions, or by RT-qPCR.

### Western blots

Cells were lysed in Radioimmunoprecipitation assay (RIPA) buffer (1% IGEPAL CA-630, 150 mM NaCl, 0.1% sodium dodecyl sulfate [SDS], 50 mM Tris pH 8.0, 1 mM Ethylenediaminetetraacetic acid (EDTA), 0.5% sodium deoxycholate) and protease inhibitor cocktail supplement (Roche, 11836170001). Protein concentration was determined by bicinchoninic acid assay (Pierce, 23227). 5 $\times$  SDS loading buffer (235 mM SDS, 10%  $\beta$ -mercaptoethanol, 0.005% bromophenol blue, 210 mM Tris-HCl pH 6.8, 50% glycerol) was added to lysates to a final 1 $\times$  concentration and incubated for 10 min at 90°C. Proteins were then resolved by SDS-polyacrylamide gel electrophoresis and transferred onto



a nitrocellulose membrane. Membranes were blocked using Odyssey Blocking Buffer (LI-COR Biosciences, P/N 927-40000). Antibodies used: anti-Cas9 (Diagenode, C15200229, 1:10,000) and anti-ERK (Cell Signaling Technologies, 4695S, 1:1000). Secondary antibodies used: anti-rabbit (LI-COR Biosciences, 926-32213, 1:10,000) and anti-mouse (LI-COR Biosciences, 926-32210, 1:10,000). Membranes were visualised using a LI-COR Odyssey CLx Infrared Imager.

## eRNA and mRNA analysis

Patient tissue ATAC-seq data processing was performed as described previously ([Britton et al., 2017](#)). Reads were mapped to GRCh38 (hg38) using Bowtie2 v2.3.0 ([Langmead and Salzberg, 2012](#)) with the following options: -X 2000 -dovetail. Mapped reads ( $\geq q30$ ) were retained using SAMtools ([Li et al., 2009](#)). Reads mapping to blacklisted regions were removed using BEDtools ([Quinlan and Hall, 2010](#)). Peaks were called using MACS2 v2.1.1 ([Zhang et al., 2008](#)) with the following parameters: -q 0.01, -nomodel-shift -75 -extsize 150 -B -SPMR. A custom union peakset was formed from all BO and OAC patient samples, using HOMER v4.9 mergePeaks.pl -d 250 ([Heinz et al., 2010](#)) as described previously ([Rogerson et al., 2019](#)) and filtered to retain only intergenic regions  $\geq 2$  kb upstream from a TSS or  $\geq 500$  bp downstream from a TTS.

RNA-seq reads were mapped to the human genome GRCh38 (hg38) using STAR v2.3.0 ([Dobin et al., 2013](#)). The expression threshold for eRNAs was determined using an adapted method from [Zhang et al., 2019](#). Briefly, total RNA-seq reads were integrated into genomic regions from the intergenic patient ATAC-seq peakset. Putative eRNA and mRNA read counts were determined using featureCounts ([Liao et al., 2014](#)) and FPM values determined using DESeq2 ([Love et al., 2014](#)). Putative eRNA regions with average counts and FPM values of  $\geq 3$  and 1.5, respectively, were taken forward for further analysis. Differentially expressed eRNAs and mRNAs were determined using DESeq2 ([Love et al., 2014](#)). For eRNAs, a  $\log_2$ -fold change of  $\pm 0.5$  and  $p\text{-value}_{\text{adj}} < 0.05$  defined differential expression. For BO and OAC mRNAs, a  $\log_2$ -fold change of  $\pm 0.9$  and  $\pm 1.5$ , respectively, and  $p\text{-value}_{\text{adj}} < 0.05$  defined differential expression. ERBB2-positive OAC samples ( $ERBB2^{\text{AMP}}$ ) were determined based on these samples having expression of *ERBB2* greater than the median *ERBB2* expression + 2 SD. Morpheus (<https://software.broadinstitute.org/morpheus/>) was used to generate heatmaps and perform hierarchical clustering.

HOMER v4.9 was used for de novo transcription factor motif enrichment analysis. To analyse footprinting signatures at putative eRNA regions, TOBIAS v0.5.1 was used ([Bentsen et al., 2020](#)). eRNAs were annotated to genes by the nearest gene model and assessed for CpG content using HOMER v4.9. Super enhancers were identified using HOMER v4.9 findPeaks.pl -style super. Net enhancer activity was calculated as in [Bi et al., 2020](#). Briefly, neighbouring genes of eRNA regions in both BO and OAC were identified and stratified into nine groups based on the net eRNA change within 200 kb of the TSS of each gene: + (or -1) stands for 1 net gained (or lost) eRNA from BO to OAC. Bidirectionality score was calculated using HOMER v4.9 analyzeRepeats.pl with the -strand option applied for each strand and score defined as  $\log_{10}((+\text{strand expression score} + 1)/(-\text{strand expression score} + 1)) + 1$ .

## DepMap data

Batch-corrected genome-wide CRISPR-Cas9 knockout screen data (DepMap Public 21Q4 CRISPR\_gene\_dependency.csv) were obtained from DepMap (<https://depmap.org/portal/>).

## ChIP-seq data analysis

ChIP-seq analysis was carried out as described previously ([Wiseman et al., 2015](#)). OE19 H3K27ac and GAC H3K4me1/3 ChIP-seq reads were mapped to the human genome GRCh38 (hg38) using Bowtie2 v2.3.0 ([Langmead and Salzberg, 2012](#)). Biological replicates were checked for concordance ( $r > 0.80$ ). Peaks were called using MACS2 v2.1.1, using input DNA as control ([Zhang et al., 2008](#)). Mapped reads ( $\geq q30$ ) were retained using SAMtools ([Li et al., 2009](#)). Reads mapping to blacklisted regions were removed using BEDtools ([Quinlan and Hall, 2010](#)).

## CUT&Tag processing and data analysis

CUT&Tag library generation was performed as described previously ([Kaya-Okur et al., 2020](#)) with an altered nuclear extraction step. For the nuclear extraction, OE19 cells were initially lysed in Nuclei

EZ lysis buffer (Sigma-Aldrich, NUC-101) at 4°C for 10 min followed by centrifugation at  $500 \times g$  for 5 min. The subsequent clean-up was performed in a buffer composed of 10 mM Tris-HCl pH 8.0, 10 mM NaCl and 0.2% NP40 followed by centrifugation at  $1300 \times g$  for 5 min. Nuclei were then lightly cross-linked in 0.1% formaldehyde for 2 min followed by quenching with 75 mM glycine followed by centrifugation at  $500 \times g$  for 5 min. Cross-linked nuclei were resuspended in 20 mM N-2-hydroxyethylpiperazine-N'-2-ethanesulfonic acid (HEPES) pH 7.5, 150 mM NaCl, and 0.5 M spermidine at a concentration of  $4\text{--}8 \times 10^3 / \mu\text{l}$  ( $2\text{--}4 \times 10^4$  total). Subsequent stages were as previously described (Kaya-Okur *et al.*, 2020). For  $2\text{--}4 \times 10^4$  nuclei, 0.5  $\mu\text{g}$  of primary and secondary antibodies were used with 1  $\mu\text{l}$  of pA-Tn5 (Epiccypher, 15-1017). Antibodies used: anti-BRD4 (abcam, ab128874), anti-CTCF (Merck-Millipore, 07-729), anti-H3K27ac (abcam, ab4729), anti-H3K27me3 (Merck-Millipore, 07-449), anti-H3K4me1 (abcam, ab8895), anti-H3K4me2 (Diagenode, pAb-035-010), anti-H3K4me3 (abcam, ab8580), anti-H3K36me3 (Diagenode, pAb-058-010), anti-H4K20me1 (Diagenode, mAb-147-010), anti-PolIII (abcam, ab817), anti-PolIII-S2 (abcam, ab5095), anti-PolIII-S5 (abcam, ab5131), and anti-Med1 (AntibodyOnline, A98044/10 UG). CUT&Tag libraries were pooled and sequenced on an Illumina HiSeq 4000 System (University of Manchester Genomic Technologies Core Facility). CUT&Tag data processing was performed as for ChIP-seq but with the MACS2 v2.1.1 (Zhang *et al.*, 2008) but the `--broad` peak calling option was used for the H4K20me1, H3K27me3 and H3K36me3 marks. Fraction reads in peak (FRiP) scores for each mark were calculated using featureCounts and a stringent threshold of  $\geq 2\%$  was set to ensure quality of data for downstream analyses (Landt *et al.*, 2012; FRiP scores are listed in *Supplementary file 12*).

ChromHMM (Ernst and Kellis, 2012) was used to train an eight-state HMM using the CUT&Tag data for all marks assayed. The number of states was determined by running the model with increasing numbers of states until state separation was observed. Emission states were annotated in accordance with Roadmap Epigenomics Consortium Data (Kundaje *et al.*, 2015).

## KAS-seq processing and data analysis

KAS-seq library generation was performed as described previously (Wu *et al.*, 2020) except with nuclear extraction and labelling reactions. Nuclei were extracted and washed as described for CUT&Tag. Nuclei were then resuspended in nuclease-free H<sub>2</sub>O at a concentration of  $1 \times 10^4 / \mu\text{l}$  ( $2 \times 10^5$  total). Labelling reactions were carried out in DNA LoBind tubes (Eppendorf, 0030108051) using 5 mM N<sub>3</sub>-kethoxal (a gift from Chuan He) in phosphate-buffered saline to a final volume of 50  $\mu\text{l}$  for 15 min at 37°C with 1000 RPM mixing in a thermomixer. Labelled gDNA was isolated using the PureLink Genomic DNA Mini kit (Thermo Fisher Scientific, K182001) and eluted twice with 21.5  $\mu\text{l}$  25 mM K<sub>3</sub>BO<sub>3</sub> pH 7.0. Subsequent library preparation stages were as previously described (Wu *et al.*, 2020). KAS-seq libraries were pooled and sequenced on an Illumina HiSeq 4000 System (University of Manchester Genomic Technologies Core Facility). Three biological replicates were sequenced and checked for concordance ( $r > 0.80$ ). KAS-seq data processing was performed as described previously (Wu *et al.*, 2020), but with the MACS2 v2.1.1 `--broad` peak calling option.

## HiC analysis

HiC samples for mammalian cells were carried out using the Arima-HiC Kit (A510008, ARIMA Genomics) with some modifications. Briefly, the nuclei were prepared from 3 million cross-linked cells ( $-80^\circ\text{C}$ ) using Nuclei EZ prep (NUC101, Sigma-Aldrich) at 4°C for 10 min and spun down  $500 \times g$  at 1°C for 5 min. The nuclei wash was carried out in 0.09% bovine serum albumin (BSA)/CapC lysis buffer (10 mM Tris-Cl pH 8.0, 10 mM NaCl, 0.2% NP40, 0.09% BSA, and 1 tablet of EDTA-free protease inhibitor cocktail (11873580001, Roche) per 50 ml) at 4°C for 10 min and spun down at  $500 \times g$  at 1°C for 5 min. The nuclei pellets were resuspended in 25  $\mu\text{l}$  of nuclease-free H<sub>2</sub>O (total volume of nuclei is  $\sim 30 \mu\text{l}$ ). A 20- $\mu\text{l}$  solution ( $\sim 2$  million) of freshly prepared nuclei was used for HiC sample preparation.

HiC libraries were generated using the Arima Library Prep module (A303011, ARIMA Genomics) as described by the manufacturers and sequenced using a NovaSeq6000 (Illumina). We used Illumina 150 bp paired end sequencing (300 cycle) to obtain  $\sim 1$  billion read-pairs per sample.

The HiC dataset consists of the two biological replicated samples in OE19 cells. The paired-end reads of each sample were aligned to the human genome hg38 by the aligning software BWA-MEM v0.7.17 (Li and Durbin, 2010). The uniquely mapped reads were processed by the HiC data analysis pipeline Juicer v1.6 (Durand *et al.*, 2016). The contacts identified in each of the two samples were

stored in the.hic files. We applied the R package HiCRep with the default settings (Yang *et al.*, 2017) to the contacts at MAPQ  $\geq 30$  to calculate the stratum-adjusted correlation coefficient (SCC) between the two replicates. As HiCRep calculated the SCC for the contacts on each chromosome, we calculated the chromosome-length weighted average of the SCCs on all the chromosomes as a summary SCC. The summary SCC for the two replicates is 0.965. We also applied the Juicer pipeline to the pool of the aligned reads from the two replicates and obtained the contacts from the merged reads of the two replicates.

The HiC data files of the two samples were uploaded in ArrayExpress repository with the ArrayExpress data ID E-MTAB-12664.

## The Cancer Genome Atlas data

Diagnosis age and overall survival between OAC patients with high or low *JUP*, *CCNE1*, and *MYBL2* RNA expression (defined as  $\pm 1$  SD from the median expression) in the TCGA PanCancer Atlas dataset (Liu *et al.*, 2018) were downloaded from cBioPortal ([https://www.cbioportal.org/study/summary?id=esca\\_tcga\\_pan\\_can\\_atlas\\_2018](https://www.cbioportal.org/study/summary?id=esca_tcga_pan_can_atlas_2018)). Oncoprint plot of mutational co-occurrence between *JUP* and *ERBB2* in OAC was generated using cBioPortal.

To establish the prognostic model, univariate Cox regression was performed using the survival package in R v3.6.0 to select genes associated with patient prognosis utilising a criteria of  $q$ -value  $< 0.1$ . A random forest algorithm was applied using the randomForestSRC package in R v3.6.0 for feature reduction to obtain a survival signature. Risk score (risk score =  $\sum x_i \times \beta_i$  where  $x_i$  is gene expression value;  $\beta_i$  is coefficient index) was calculated using a multivariate Cox regression model. Patients were grouped by the median value of risk score and Kaplan–Meier analysis performed to compare the survival difference between high- and low-risk score group. Visualisation was achieved using the survminer package in R v3.6.0.

## Bioinformatics

Genome browser data were visualised using the UCSC Genome Browser (Kent *et al.*, 2002). Heatmaps and tag density plots of epigenomic data were generated the using deepTools (Ramírez *et al.*, 2016) computeMatrix, plotProfile, plotCorrelation, and plotHeatmap functions. Metascape (Zhou *et al.*, 2019) was used for GO analysis of gene sets. The eulerr package in R v3.6.0 was used for generating Venn diagrams.

## Datasets

All data were obtained from ArrayExpress, unless stated otherwise. Human tissue RNA-seq data were obtained from: OCCAMS consortium (European Genome-Phenome Archive, EGAD00001007496). Human tissue ATAC-seq data were obtained from: E-MTAB-5169 (Britton *et al.*, 2017), E-MTAB-6751 (Rogerson *et al.*, 2019), and E-MTAB-8447 (Rogerson *et al.*, 2020). The Cancer Genome Atlas OAC ATAC-seq data were obtained from the GDC data portal (<https://portal.gdc.cancer.gov/>; Corces *et al.*, 2018). OE19 H3K27ac ChIP-seq was obtained from: E-MTAB-10319 (Ogden *et al.*, 2022). GAC H3K4me1 and H3K4me3 ChIP-seq were obtained from: Gene Expression Omnibus, GSE75898 (Ooi *et al.*, 2016). OE19 siKLF5 RNA-seq and KLF5 ChIP-seq were obtained from: E-MTAB-8446 and E-MTAB-8568, respectively (Rogerson *et al.*, 2020). OE19 dnFOS RNA-seq was obtained from E-MTAB-10334 (Ogden *et al.*, 2023).

## Data access

All data have been deposited at ArrayExpress; OE19 KAS-seq and CUT&Tag data (E-MTAB-11357 and E-MTAB-11356, respectively), and OE19 HiC data (E-MTAB-12664).

## Acknowledgements

We thank Guanhua Yan for excellent technical assistance, and staff in the Bioinformatics, and Genomic Technologies core facilities. We also thank Nicoletta Bobola and Sankari Nagarajan, for critical appraisal of the manuscript. We thank all lab members, Hannah Reed and Connor Rogerson for experimental and analytical advice. We are grateful to Chuan He for providing N<sub>3</sub>-kethoxal. This work was funded by grants to ADS from the MRC (MR/V010263/1) and the Wellcome Trust (102171/B/13/Z).

## Additional information

### Competing interests

The OCCAMs consortium: The other authors declare that no competing interests exist.

### Funding

Funder	Grant reference number	Author
Medical Research Council	MR/V010263/1	Shen-Hsi Yang
Wellcome Trust	102171/B/13/Z	Ibrahim Ahmed

The funders had no role in study design, data collection, and interpretation, or the decision to submit the work for publication. For the purpose of Open Access, the authors have applied a CC BY public copyright license to any Author Accepted Manuscript version arising from this submission.

### Author contributions

Ibrahim Ahmed, Formal analysis, Investigation, Methodology, Writing - original draft, Writing - review and editing; Shen-Hsi Yang, Formal analysis, Supervision, Investigation, Writing - review and editing; Samuel Ogden, Wei Zhang, Formal analysis, Investigation, Writing - review and editing; Yaoyong Li, Formal analysis; The OCCAMs consortium, Resources; Andrew D Sharrocks, Conceptualization, Supervision, Funding acquisition, Writing - original draft, Project administration, Writing - review and editing

### Author ORCIDs

Ibrahim Ahmed  <http://orcid.org/0000-0002-7424-6658>

Samuel Ogden  <http://orcid.org/0000-0002-0217-881X>

Andrew D Sharrocks  <http://orcid.org/0000-0001-7395-9552>

### Decision letter and Author response

Decision letter <https://doi.org/10.7554/eLife.80840.sa1>

Author response <https://doi.org/10.7554/eLife.80840.sa2>

---

## Additional files

### Supplementary files

- Supplementary file 1. All expressed eRNAs identified in Barrett's and OAC samples.
- Supplementary file 2. eRNAs upregulated in OAC.
- Supplementary file 3. eRNAs upregulated in Barrett's.
- Supplementary file 4. KAS-seq peaks in OE19 cells.
- Supplementary file 5. Super enhancers.
- Supplementary file 6. Motif enrichment.
- Supplementary file 7. BINDetect scores.
- Supplementary file 8. Genes upregulated in OAC.
- Supplementary file 9. Genes upregulated in Barrett's.
- Supplementary file 10. Genes associated with eRNA regions.
- Supplementary file 11. PCR primer and sgRNA sequences.
- Supplementary file 12. CUT&Tag FRIP scores.
- MDAR checklist

### Data availability

All data have been deposited at ArrayExpress; OE19 KAS-seq and CUT&TAG data (E-MTAB-11357 and E-MTAB-11356, respectively) and OE19 HiC data (E-MTAB-12664).

The following datasets were generated:

Author(s)	Year	Dataset title	Dataset URL	Database and Identifier
Ahmed I, Yang SH, Ogden S, Zhang W, Li Y, Sharrocks AD, OCCAMS Consortium	2022	KAS-seq in OE19 cells	<a href="https://www.ebi.ac.uk/arrayexpress/experiments/E-MTAB-11357">https://www.ebi.ac.uk/arrayexpress/experiments/E-MTAB-11357</a>	ArrayExpress, E-MTAB-11357
Ahmed I, Yang SH, Ogden S, Zhang W, Li Y, Sharrocks AD, OCCAMS Consortium	2022	CUT&TAG of OE19 cell line	<a href="https://www.ebi.ac.uk/arrayexpress/experiments/E-MTAB-11356">https://www.ebi.ac.uk/arrayexpress/experiments/E-MTAB-11356</a>	ArrayExpress, E-MTAB-11356
Ahmed I, Yang SH, Ogden S, Zhang W, Li Y, Sharrocks AD, OCCAMS Consortium	2023	HiC data in OE19 cells	<a href="http://www.ebi.ac.uk/arrayexpress/experiments/E-MTAB-12664">http://www.ebi.ac.uk/arrayexpress/experiments/E-MTAB-12664</a>	ArrayExpress, E-MTAB-12664

The following previously published datasets were used:

Author(s)	Year	Dataset title	Dataset URL	Database and Identifier
Ooi WF, Xing M, Xu C, Yao X, Ramlee MK, Lim MC, Cao F, Lim K, Babu D, Poon LF, Lin Suling J, Qamra A, Irwanto A, Qu Zhengzhong J, Nandi T, Lee-Lim AP, Chan YS, Tay ST, Lee MH, Davies JO, Wong WK, Soo KC, Chan WH, Ong HS, Chow P, Wong CY, Rha SY, Liu J, Hillmer AM, Hughes JR, Rozen S, Teh BT, Fullwood MJ, Li S, Tan P	2016	Somatic Promoter Landscape of Primary Gastric Adenocarcinoma Delineated by Epigenomic Profiling	<a href="https://www.ncbi.nlm.nih.gov/geo/query/acc.cgi?acc=GSE75898">https://www.ncbi.nlm.nih.gov/geo/query/acc.cgi?acc=GSE75898</a>	NCBI Gene Expression Omnibus, GSE75898
Ogden S, Carys K, Bruce J, The OCCAMS Consortium, Sharrocks AD	2021	Sequencing data for oesophageal and related samples - Ogden et al release	<a href="https://ega-archive.org/datasets/EGAD00001007496">https://ega-archive.org/datasets/EGAD00001007496</a>	European Genome Phenome Archive, EGAD00001007496
Britton E, Rogerson C, Mehta S, Li Y, Li X, Fitzgerald RC, Ang YS, Sharrocks AD	2017	ATAC-seq of oesophageal cell lines and tissue samples	<a href="https://www.ebi.ac.uk/arrayexpress/experiments/E-MTAB-5169">https://www.ebi.ac.uk/arrayexpress/experiments/E-MTAB-5169</a>	ArrayExpress, E-MTAB-5169
Rogerson C, Britton E, Withey S, Hanley N, Ang YS, Sharrocks AD	2019	ATAC-seq of human Barrett's oesophagus tissue	<a href="https://www.ebi.ac.uk/arrayexpress/experiments/E-MTAB-6751">https://www.ebi.ac.uk/arrayexpress/experiments/E-MTAB-6751</a>	ArrayExpress, E-MTAB-6751
Rogerson C, Britton E, Withey S, Hanley N, Ang YS, Sharrocks AD	2020	ATAC-seq of oesophageal adenocarcinoma patient samples	<a href="https://www.ebi.ac.uk/arrayexpress/experiments/E-MTAB-8447">https://www.ebi.ac.uk/arrayexpress/experiments/E-MTAB-8447</a>	ArrayExpress, E-MTAB-8447
Rogerson C, Ogden S, Britton E, OCCAMS Consortium, Ang YS, Sharrocks AD	2020	RNA-seq of OE19 cells treated with siNT or siKLF5 for 72 hours	<a href="https://www.ebi.ac.uk/arrayexpress/experiments/E-MTAB-8446">https://www.ebi.ac.uk/arrayexpress/experiments/E-MTAB-8446</a>	ArrayExpress, E-MTAB-8446
Rogerson C, Ogden S, Britton E, OCCAMS Consortium, Ang YS, Sharrocks AD	2020	KLF5 ChIP-seq in CP-A and OE19 cells	<a href="https://www.ebi.ac.uk/arrayexpress/experiments/E-MTAB-8568">https://www.ebi.ac.uk/arrayexpress/experiments/E-MTAB-8568</a>	ArrayExpress, E-MTAB-8568

*Continued on next page*

Continued

Author(s)	Year	Dataset title	Dataset URL	Database and Identifier
Ogden S, Ahmed I, Yang S-H, Fullwood P, The OCCAMS Consortium, Francavilla C, Sharrocks AD	2023	OE19 dnFOS RNA-seq	<a href="https://www.ebi.ac.uk/arrayexpress/experiments/E-MTAB-10334">https://www.ebi.ac.uk/arrayexpress/experiments/E-MTAB-10334</a>	ArrayExpress, E-MTAB-10334
Ogden S, Carys K, Bruce J, The OCCAMS Consortium, Sharrocks AD	2021	ChIP-seq of H3K27Ac in oesophageal adenocarcinoma OE19 cells	<a href="https://www.ebi.ac.uk/arrayexpress/experiments/E-MTAB-10319">https://www.ebi.ac.uk/arrayexpress/experiments/E-MTAB-10319</a>	ArrayExpress, E-MTAB-10319
Corces MR, Granja JM, Shams S, Louie BH, Seoane JA, Zhou W, Silva TC, Groeneveld C, Wong CK, Cho SW, Satpathy AT, Mumbach MR, Hoadley KA, Robertson AG, Sheffield NC, Felau I, Castro MAA, Berman BP, Staudt LM, Zenklusen JC, Laird PW, Curtis C, Cancer Genome Atlas Analysis Network, Greenleaf WJ, Chang HY	2018	TCGA-generated ATAC-seq of oesophageal adenocarcinoma patient samples	<a href="https://gdc.cancer.gov/about-data/publications/ATACseq-AWG">https://gdc.cancer.gov/about-data/publications/ATACseq-AWG</a>	NIH GDC, ATAC-AWG

## References

- Aktary Z**, Alaei M, Pasdar M. 2017. Beyond cell-cell adhesion: plakoglobin and the regulation of tumorigenesis and metastasis. *Oncotarget* **8**:32270–32291. DOI: <https://doi.org/10.18632/oncotarget.15650>, PMID: [28416759](https://pubmed.ncbi.nlm.nih.gov/28416759/)
- Andersson R**, Gebhard C, Miguel-Escalada I, Hoof I, Bornholdt J, Boyd M, Chen Y, Zhao X, Schmidl C, Suzuki T, Ntini E, Arner E, Valen E, Li K, Schwarzfischer L, Glatz D, Raithel J, Lilje B, Rapin N, Bagger FO, et al. 2014. An atlas of active enhancers across human cell types and tissues. *Nature* **507**:455–461. DOI: <https://doi.org/10.1038/nature12787>, PMID: [24670763](https://pubmed.ncbi.nlm.nih.gov/24670763/)
- Andersson R**, Sandelin A. 2020. Determinants of enhancer and promoter activities of regulatory elements. *Nature Reviews. Genetics* **21**:71–87. DOI: <https://doi.org/10.1038/s41576-019-0173-8>, PMID: [31605096](https://pubmed.ncbi.nlm.nih.gov/31605096/)
- Arnold CD**, Gerlach D, Stelzer C, Boryn ŁM, Rath M, Stark A. 2013. Genome-Wide quantitative enhancer activity maps identified by STARR-seq. *Science* **339**:1074–1077. DOI: <https://doi.org/10.1126/science.1232542>, PMID: [23328393](https://pubmed.ncbi.nlm.nih.gov/23328393/)
- Bang YJ**, Van Cutsem E, Feyereislova A, Chung HC, Shen L, Sawaki A, Lordick F, Ohtsu A, Omuro Y, Satoh T, Aprile G, Kulikov E, Hill J, Lehle M, Rüschoff J, Kang YK, ToGA Trial Investigators. 2010. Trastuzumab in combination with chemotherapy versus chemotherapy alone for treatment of HER2-positive advanced gastric or gastro-oesophageal junction cancer (toga): a phase 3, open-label, randomised controlled trial. *Lancet* **376**:687–697. DOI: [https://doi.org/10.1016/S0140-6736\(10\)61121-X](https://doi.org/10.1016/S0140-6736(10)61121-X), PMID: [20728210](https://pubmed.ncbi.nlm.nih.gov/20728210/)
- Behan FM**, Iorio F, Picco G, Gonçalves E, Beaver CM, Migliardi G, Santos R, Rao Y, Sassi F, Pinnelli M, Ansari R, Harper S, Jackson DA, McRae R, Pooley R, Wilkinson P, van der Meer D, Dow D, Buser-Doepner C, Bertotti A, et al. 2019. Prioritization of cancer therapeutic targets using CRISPR-Cas9 screens. *Nature* **568**:511–516. DOI: <https://doi.org/10.1038/s41586-019-1103-9>, PMID: [30971826](https://pubmed.ncbi.nlm.nih.gov/30971826/)
- Bentsen M**, Goymann P, Schultheis H, Klee K, Petrova A, Wiegandt R, Fust A, Preussner J, Kuenne C, Braun T, Kim J, Looso M. 2020. Atac-seq footprinting unravels kinetics of transcription factor binding during zygotic genome activation. *Nature Communications* **11**:4267. DOI: <https://doi.org/10.1038/s41467-020-18035-1>, PMID: [32848148](https://pubmed.ncbi.nlm.nih.gov/32848148/)
- Bi M**, Zhang Z, Jiang Y-Z, Xue P, Wang H, Lai Z, Fu X, De Angelis C, Gong Y, Gao Z, Ruan J, Jin VX, Marangoni E, Montaudon E, Glass CK, Li W, Huang TH-M, Shao Z-M, Schiff R, Chen L, et al. 2020. Enhancer reprogramming driven by high-order assemblies of transcription factors promotes phenotypic plasticity and breast cancer endocrine resistance. *Nature Cell Biology* **22**:701–715. DOI: <https://doi.org/10.1038/s41556-020-0514-z>, PMID: [32424275](https://pubmed.ncbi.nlm.nih.gov/32424275/)

- Bolger AM**, Lohse M, Usadel B. 2014. Trimmomatic: a flexible trimmer for illumina sequence data. *Bioinformatics* **30**:2114–2120. DOI: <https://doi.org/10.1093/bioinformatics/btu170>, PMID: 24695404
- Britton E**, Rogerson C, Mehta S, Li Y, Li X, OCCAMS consortium, Fitzgerald RC, Ang YS, Sharrocks AD. 2017. Open chromatin profiling identifies AP1 as a transcriptional regulator in oesophageal adenocarcinoma. *PLoS Genetics* **13**:e1006879. DOI: <https://doi.org/10.1371/journal.pgen.1006879>, PMID: 28859074
- Cancer Genome Atlas Research Network**, Analysis Working Group: Asan University, BC Cancer Agency, Brigham and Women's Hospital, Broad Institute, Brown University, Case Western Reserve University, Dana-Farber Cancer Institute, Duke University, Greater Poland Cancer Centre, Harvard Medical School, Institute for Systems Biology, KU Leuven, Mayo Clinic, Memorial Sloan Kettering Cancer Center, National Cancer Institute, Nationwide Children's Hospital, Stanford University, University of Alabama, University of Michigan, University of North Carolina, University of Pittsburgh, University of Rochester, University of Southern California, University of Texas MD Anderson Cancer Center, University of Washington, Van Andel Research Institute, Vanderbilt University, Washington University, Genome Sequencing Center: Broad Institute, Washington University in St. Louis, Genome Characterization Centers: BC Cancer Agency, Broad Institute, Harvard Medical School, Sidney Kimmel Comprehensive Cancer Center at Johns Hopkins University, University of North Carolina, University of Southern California Epigenome Center, University of Texas MD Anderson Cancer Center, Van Andel Research Institute, Genome Data Analysis Centers: Broad Institute, Brown University, Harvard Medical School, Institute for Systems Biology, Memorial Sloan Kettering Cancer Center, University of California Santa Cruz, University of Texas MD Anderson Cancer Center, Biospecimen Core Resource: International Genomics Consortium, Research Institute at Nationwide Children's Hospital, Tissue Source Sites: Analytic Biologic Services, Asan Medical Center, Asterand Bioscience, Barretos Cancer Hospital, BioreclamationIVT, Botkin Municipal Clinic, Chonnam National University Medical School, Christiana Care Health System, Cureline, Duke University, Emory University, Erasmus University, Indiana University School of Medicine, Institute of Oncology of Moldova, International Genomics Consortium, Invidumed, Israelitisches Krankenhaus Hamburg, Keimyung University School of Medicine, Memorial Sloan Kettering Cancer Center, National Cancer Center Goyang, Ontario Tumour Bank, Peter MacCallum Cancer Centre, Pusan National University Medical School, Ribeirão Preto Medical School, St. Joseph's Hospital & Medical Center, St. Petersburg Academic University, Tayside Tissue Bank, University of Dundee, University of Kansas Medical Center, University of Michigan, University of North Carolina at Chapel Hill, University of Pittsburgh School of Medicine, University of Texas MD Anderson Cancer Center, Disease Working Group: Duke University, Memorial Sloan Kettering Cancer Center, National Cancer Institute, University of Texas MD Anderson Cancer Center, Yonsei University College of Medicine, Data Coordination Center: CSRA Inc, Project Team: National Institutes of Health. 2017. Integrated genomic characterization of oesophageal carcinoma. *Nature* **541**:169–175. DOI: <https://doi.org/10.1038/nature20805>, PMID: 28052061
- Chen H**, Li C, Peng X, Zhou Z, Weinstein JN, Cancer Genome Atlas Research Network, Liang H. 2018. A pan-cancer analysis of enhancer expression in nearly 9000 patient samples. *Cell* **173**:386–399. DOI: <https://doi.org/10.1016/j.cell.2018.03.027>, PMID: 29625054
- Chen L**, Huang M, Plummer J, Pan J, Jiang YY, Yang Q, Silva TC, Gull N, Chen S, Ding LW, An O, Yang H, Cheng Y, Said JW, Doan N, Dinjens WN, Waters KM, Tuli R, Gayther SA, Klemperer SJ, et al. 2020. Master transcription factors form interconnected circuitry and orchestrate transcriptional networks in oesophageal adenocarcinoma. *Gut* **69**:630–640. DOI: <https://doi.org/10.1136/gutjnl-2019-318325>, PMID: 31409603
- Coleman HG**, Xie SH, Lagergren J. 2018. The epidemiology of esophageal adenocarcinoma. *Gastroenterology* **154**:390–405. DOI: <https://doi.org/10.1053/j.gastro.2017.07.046>, PMID: 28780073
- Corces MR**, Granja JM, Shams S, Louie BH, Seoane JA, Zhou W, Silva TC, Groeneveld C, Wong CK, Cho SW, Satpathy AT, Mumbach MR, Hoadley KA, Robertson AG, Sheffield NC, Felau I, Castro MAA, Berman BP, Staudt LM, Zenklusen JC, et al. 2018. The chromatin accessibility landscape of primary human cancers. *Science* **362**:eaav1898. DOI: <https://doi.org/10.1126/science.aav1898>, PMID: 30361341
- Creyghton MP**, Cheng AW, Welstead GG, Kooistra T, Carey BW, Steine EJ, Hanna J, Lodato MA, Frampton GM, Sharp PA, Boyer LA, Young RA, Jaenisch R. 2010. Histone h3k27ac separates active from poised enhancers and predicts developmental state. *PNAS* **107**:21931–21936. DOI: <https://doi.org/10.1073/pnas.1016071107>, PMID: 21106759
- De Santa F**, Barozzi I, Mietton F, Ghisletti S, Polletti S, Tusi BK, Muller H, Ragoussis J, Wei CL, Natoli G. 2010. A large fraction of extragenic RNA Pol II transcription sites overlap enhancers. *PLoS Biology* **8**:e1000384. DOI: <https://doi.org/10.1371/journal.pbio.1000384>, PMID: 20485488
- Dobin A**, Davis CA, Schlesinger F, Drenkow J, Zaleski C, Jha S, Batut P, Chaisson M, Gingeras TR. 2013. STAR: ultrafast universal RNA-seq aligner. *Bioinformatics* **29**:15–21. DOI: <https://doi.org/10.1093/bioinformatics/bts635>, PMID: 23104886
- Durand NC**, Shamim MS, Machol I, Rao SSP, Huntley MH, Lander ES, Aiden EL. 2016. Juicer provides a one-click system for analyzing loop-resolution hi-C experiments. *Cell Systems* **3**:95–98. DOI: <https://doi.org/10.1016/j.cels.2016.07.002>, PMID: 27467249
- Ernst J**, Kellis M. 2012. ChromHMM: automating chromatin-state discovery and characterization. *Nature Methods* **9**:215–216. DOI: <https://doi.org/10.1038/nmeth.1906>, PMID: 22373907
- Frankell AM**, Jammula S, Li X, Contino G, Killcoyne S, Abbas S, Perner J, Bower L, Devonshire G, Ococks E, Grehan N, Mok J, O'Donovan M, MacRae S, Eldridge MD, Tavaré S, Clinical OC, Fitzgerald RC. 2019. The landscape of selection in 551 esophageal adenocarcinomas defines genomic biomarkers for the clinic. *Nature Genetics* **51**:506–516. DOI: <https://doi.org/10.1038/s41588-018-0331-5>, PMID: 30718927
- Heigwer F**, Kerr G, Boutros M. 2014. E-CRISP: fast CRISPR target site identification. *Nature Methods* **11**:122–123. DOI: <https://doi.org/10.1038/nmeth.2812>, PMID: 24481216

- Heintzman ND**, Stuart RK, Hon G, Fu Y, Ching CW, Hawkins RD, Barrera LO, Van Calcar S, Qu C, Ching KA, Wang W, Weng Z, Green RD, Crawford GE, Ren B. 2007. Distinct and predictive chromatin signatures of transcriptional promoters and enhancers in the human genome. *Nature Genetics* **39**:311–318. DOI: <https://doi.org/10.1038/ng1966>, PMID: 17277777
- Heinz S**, Benner C, Spann N, Bertolino E, Lin YC, Laslo P, Cheng JX, Murre C, Singh H, Glass CK. 2010. Simple combinations of lineage-determining transcription factors prime cis-regulatory elements required for macrophage and B cell identities. *Molecular Cell* **38**:576–589. DOI: <https://doi.org/10.1016/j.molcel.2010.05.004>, PMID: 20513432
- Hnisz D**, Abraham BJ, Lee TI, Lau A, Saint-André V, Sigova AA, Hoke HA, Young RA. 2013. Super-Enhancers in the control of cell identity and disease. *Cell* **155**:934–947. DOI: <https://doi.org/10.1016/j.cell.2013.09.053>, PMID: 24119843
- Hsieh CL**, Fei T, Chen Y, Li T, Gao Y, Wang X, Sun T, Sweeney CJ, Lee GSM, Chen S, Balk SP, Liu XS, Brown M, Kantoff PW. 2014. Enhancer RNAs participate in androgen receptor-driven looping that selectively enhances gene activation. *PNAS* **111**:7319–7324. DOI: <https://doi.org/10.1073/pnas.1324151111>, PMID: 24778216
- Hu Q**, Kwon YS, Nunez E, Cardamone MD, Hutt KR, Ohgi KA, Garcia-Bassets I, Rose DW, Glass CK, Rosenfeld MG, Fu XD. 2008. Enhancing nuclear receptor-induced transcription requires nuclear motor and LSD1-dependent gene networking in interchromatin granules. *PNAS* **105**:19199–19204. DOI: <https://doi.org/10.1073/pnas.0810634105>, PMID: 19052240
- Huang J**, Liu X, Li D, Shao Z, Cao H, Zhang Y, Trompouki E, Bowman TV, Zou LI, Yuan GC, Orkin SH, Xu J. 2016. Dynamic control of enhancer repertoires drives lineage and stage-specific transcription during hematopoiesis. *Developmental Cell* **36**:9–23. DOI: <https://doi.org/10.1016/j.devcel.2015.12.014>, PMID: 26766440
- Hung KL**, Yost KE, Xie L, Shi Q, Helmsauer K, Luebeck J, Schöpflin R, Lange JT, Chamorro González R, Weiser NE, Chen C, Valieva ME, Wong IT-L, Wu S, Dehkordi SR, Duffy CV, Kraft K, Tang J, Belk JA, Rose JC, et al. 2021. EcDNA hubs drive cooperative intermolecular oncogene expression. *Nature* **600**:731–736. DOI: <https://doi.org/10.1038/s41586-021-04116-8>, PMID: 34819668
- Jammula S**, Katz-Summercorn AC, Li X, Linossi C, Smyth E, Killcoyne S, Biasci D, Subash VV, Abbas S, Blasko A, Devonshire G, Grantham A, Wronowski F, O'Donovan M, Grehan N, Eldridge MD, Tavaré S, Fitzgerald RC, Oesophageal Cancer Clinical and Molecular Stratification consortium. 2020. Identification of subtypes of Barrett's esophagus and esophageal adenocarcinoma based on DNA methylation profiles and integration of transcriptome and genome data. *Gastroenterology* **158**:1682–1697. DOI: <https://doi.org/10.1053/j.gastro.2020.01.044>, PMID: 32032585
- Kaya-Okur HS**, Janssens DH, Henikoff JG, Ahmad K, Henikoff S. 2020. Efficient low-cost chromatin profiling with cut & tag. *Nature Protocols* **15**:3264–3283. DOI: <https://doi.org/10.1038/s41596-020-0373-x>, PMID: 32913232
- Kent WJ**, Sugnet CW, Furey TS, Roskin KM, Pringle TH, Zahler AM, Haussler D. 2002. The human genome browser at UCSC. *Genome Research* **12**:996–1006. DOI: <https://doi.org/10.1101/gr.229102>, PMID: 12045153
- Kim TK**, Hemberg M, Gray JM, Costa AM, Bear DM, Wu J, Harmin DA, Laptewicz M, Barbara-Haley K, Kuersten S, Markenscoff-Papadimitriou E, Kuhl D, Bito H, Worley PF, Kreiman G, Greenberg ME. 2010. Widespread transcription at neuronal activity-regulated enhancers. *Nature* **465**:182–187. DOI: <https://doi.org/10.1038/nature09033>, PMID: 20393465
- Kundaje A**, Meuleman W, Ernst J, Bilenky M, Yen A, Heravi-Moussavi A, Kheradpour P, Zhang Z, Wang J, Ziller MJ, Amin V, Whitaker JW, Schultz MD, Ward LD, Sarkar A, Quon G, Sandstrom RS, Eaton ML, Wu YC, Pfenning AR, et al. 2015. Integrative analysis of 111 reference human epigenomes. *Nature* **518**:317–330. DOI: <https://doi.org/10.1038/nature14248>, PMID: 25693563
- Landt SG**, Marinov GK, Kundaje A, Kheradpour P, Pauli F, Batzoglou S, Bernstein BE, Bickel P, Brown JB, Cayting P, Chen Y, DeSalvo G, Epstein C, Fisher-Aylor KI, Euskirchen G, Gerstein M, Gertz J, Hartemink AJ, Hoffman MM, Iyer VR, et al. 2012. Chip-Seq guidelines and practices of the encode and modencode consortia. *Genome Research* **22**:1813–1831. DOI: <https://doi.org/10.1101/gr.136184.111>, PMID: 22955991
- Langmead B**, Salzberg SL. 2012. Fast gapped-read alignment with bowtie 2. *Nature Methods* **9**:357–359. DOI: <https://doi.org/10.1038/nmeth.1923>, PMID: 22388286
- Li H**, Handsaker B, Wysoker A, Fennell T, Ruan J, Homer N, Marth G, Abecasis G, Durbin R, 1000 Genome Project Data Processing Subgroup. 2009. The sequence alignment/map format and samtools. *Bioinformatics* **25**:2078–2079. DOI: <https://doi.org/10.1093/bioinformatics/btp352>, PMID: 19505943
- Li H**, Durbin R. 2010. Fast and accurate long-read alignment with burrows-wheeler transform. *Bioinformatics* **26**:589–595. DOI: <https://doi.org/10.1093/bioinformatics/btp698>, PMID: 20080505
- Li W**, Hu Y, Oh S, Ma Q, Merkurjev D, Song X, Zhou X, Liu Z, Tanasa B, He X, Chen AY, Ohgi K, Zhang J, Liu W, Rosenfeld MG. 2015. Condensin I and II complexes license full estrogen receptor  $\alpha$ -dependent enhancer activation. *Molecular Cell* **59**:188–202. DOI: <https://doi.org/10.1016/j.molcel.2015.06.002>, PMID: 26166704
- Liao Y**, Smyth GK, Shi W. 2014. FeatureCounts: an efficient general purpose program for assigning sequence reads to genomic features. *Bioinformatics* **30**:923–930. DOI: <https://doi.org/10.1093/bioinformatics/btt656>, PMID: 24227677
- Liu J**, Lichtenberg T, Hoadley KA, Poisson LM, Lazar AJ, Cherniack AD, Kovatich AJ, Benz CC, Levine DA, Lee AV, Omberg L, Wolf DM, Shriver CD, Thorsson V, Network CGAR, Hu H. 2018. An integrated TCGA pan-cancer clinical data resource to drive high-quality survival outcome analytics. *Cell* **173**:400–416. DOI: <https://doi.org/10.1016/j.cell.2018.02.052>, PMID: 29625055
- Love MI**, Huber W, Anders S. 2014. Moderated estimation of fold change and dispersion for RNA-seq data with DESeq2. *Genome Biology* **15**:550. DOI: <https://doi.org/10.1186/s13059-014-0550-8>, PMID: 25516281



- Maag JLV**, Fisher OM, Levert-Mignon A, Kaczorowski DC, Thomas ML, Hussey DJ, Watson DI, Wettstein A, Bobryshev YV, Edwards M, Dinger ME, Lord RV. 2017. Novel aberrations uncovered in Barrett's esophagus and esophageal adenocarcinoma using whole transcriptome sequencing. *Molecular Cancer Research* **15**:1558–1569. DOI: <https://doi.org/10.1158/1541-7786.MCR-17-0332>, PMID: 28751461
- Ng AWT**, Contino G, Killcoyne S, Devonshire G, Hsu R, Abbas S, Su J, Redmond AM, Weaver JMJ, Eldridge MD, Tavaré S, Clinical OC, Edwards PAW, Fitzgerald RC. 2022. Rearrangement processes and structural variations show evidence of selection in oesophageal adenocarcinomas. *Communications Biology* **5**:335. DOI: <https://doi.org/10.1038/s42003-022-03238-7>, PMID: 35396535
- Ogden S**, Carys K, Ahmed I, Bruce J, Sharrocks AD. 2022. Regulatory chromatin rewiring promotes metabolic switching during adaptation to oncogenic receptor tyrosine kinase inhibition. *Oncogene* **41**:4808–4822. DOI: <https://doi.org/10.1038/s41388-022-02465-w>, PMID: 36153371
- Ogden S**, Ahmed I, Yang SH, Fullwood P, consortium O, Francavilla C, Sharrocks AD. 2023. Oncogenic ERBB2 signals through the AP-1 transcription factor to control mesenchymal-like properties of oesophageal adenocarcinoma. *NAR Cancer* **5**:zcad001. DOI: <https://doi.org/10.1093/narcan/zcad001>, PMID: 36694726
- Olive M**, Krylov D, Echlin DR, Gardner K, Taparowsky E, Vinson C. 1997. A dominant negative to activation protein-1 (AP1) that abolishes DNA binding and inhibits oncogenesis. *The Journal of Biological Chemistry* **272**:18586–18594. DOI: <https://doi.org/10.1074/jbc.272.30.18586>, PMID: 9228025
- Ooi WF**, Xing M, Xu C, Yao X, Ramlee MK, Lim MC, Cao F, Lim K, Babu D, Poon LF, Lin Suling J, Qamra A, Irwanto A, Qu Zhengzhong J, Nandi T, Lee-Lim AP, Chan YS, Tay ST, Lee MH, Davies JOJ, et al. 2016. Epigenomic profiling of primary gastric adenocarcinoma reveals super-enhancer heterogeneity. *Nature Communications* **7**:12983. DOI: <https://doi.org/10.1038/ncomms12983>, PMID: 27677335
- Peters Y**, Al-Kaabji A, Shaheen NJ, Chak A, Blum A, Souza RF, Di Pietro M, Iyer PG, Pech O, Fitzgerald RC, Siersema PD. 2019. Barrett oesophagus. *Nature Reviews. Disease Primers* **5**:35. DOI: <https://doi.org/10.1038/s41572-019-0086-z>, PMID: 31123267
- Quinlan AR**, Hall IM. 2010. BEDTools: a flexible suite of utilities for comparing genomic features. *Bioinformatics* **26**:841–842. DOI: <https://doi.org/10.1093/bioinformatics/btq033>, PMID: 20110278
- Ramírez F**, Ryan DP, Grüning B, Bhardwaj V, Kilpert F, Richter AS, Heyne S, Dündar F, Manke T. 2016. DeepTools2: a next generation web server for deep-sequencing data analysis. *Nucleic Acids Research* **44**:W160–W165. DOI: <https://doi.org/10.1093/nar/gkw257>, PMID: 27079975
- R Development Core Team**. 2018. R: A language and environment for statistical computing. Vienna, Austria. R Foundation for Statistical Computing. <http://www.r-project.org>
- Ren G**, Jin W, Cui K, Rodrigez J, Hu G, Zhang Z, Larson DR, Zhao K. 2017. Ctf-Mediated enhancer-promoter interaction is a critical regulator of cell-to-cell variation of gene expression. *Molecular Cell* **67**:1049–1058. DOI: <https://doi.org/10.1016/j.molcel.2017.08.026>, PMID: 28938092
- Rogerson C**, Britton E, Withey S, Hanley N, Ang YS, Sharrocks AD. 2019. Identification of a primitive intestinal transcription factor network shared between esophageal adenocarcinoma and its precancerous precursor state. *Genome Research* **29**:723–736. DOI: <https://doi.org/10.1101/gr.243345.118>, PMID: 30962179
- Rogerson C**, Ogden S, Britton E, Consortium O, Ang Y, Sharrocks AD. 2020. Repurposing of KLF5 activates a cell cycle signature during the progression from a precursor state to oesophageal adenocarcinoma. *eLife* **9**:e57189. DOI: <https://doi.org/10.7554/eLife.57189>, PMID: 32880368
- Ross-Innes CS**, Becq J, Warren A, Cheetham RK, Northen H, O'Donovan M, Malhotra S, di Pietro M, Ivakhno S, He M, Weaver JMJ, Lynch AG, Kingsbury Z, Ross M, Humphray S, Bentley D, Fitzgerald RC. 2015. Whole-Genome sequencing provides new insights into the clonal architecture of Barrett's esophagus and esophageal adenocarcinoma. *Nature Genetics* **47**:1038–1046. DOI: <https://doi.org/10.1038/ng.3357>, PMID: 26192915
- Sanyal A**, Lajoie BR, Jain G, Dekker J. 2012. The long-range interaction landscape of gene promoters. *Nature* **489**:109–113. DOI: <https://doi.org/10.1038/nature11279>, PMID: 22955621
- Spilianakis CG**, Lalioti MD, Town T, Lee GR, Flavell RA. 2005. Interchromosomal associations between alternatively expressed loci. *Nature* **435**:637–645. DOI: <https://doi.org/10.1038/nature03574>, PMID: 15880101
- Stachler MD**, Taylor-Weiner A, Peng S, McKenna A, Agoston AT, Odze RD, Davison JM, Nason KS, Loda M, Leshchiner I, Stewart C, Stojanov P, Seepo S, Lawrence MS, Ferrer-Torres D, Lin J, Chang AC, Gabriel SB, Lander ES, Beer DG, et al. 2015. Paired exome analysis of Barrett's esophagus and adenocarcinoma. *Nature Genetics* **47**:1047–1055. DOI: <https://doi.org/10.1038/ng.3343>, PMID: 26192918
- Stemmer M**, Thumberger T, Del Sol Keyer M, Wittbrodt J, Mateo JL. 2015. CCTop: an intuitive, flexible and reliable CRISPR/Cas9 target prediction tool. *PLOS ONE* **10**:e0124633. DOI: <https://doi.org/10.1371/journal.pone.0124633>, PMID: 25909470
- Tiscornia G**, Singer O, Verma IM. 2006. Production and purification of lentiviral vectors. *Nature Protocols* **1**:241–245. DOI: <https://doi.org/10.1038/nprot.2006.37>
- Tsherniak A**, Vazquez F, Montgomery PG, Weir BA, Kryukov G, Cowley GS, Gill S, Harrington WF, Pantel S, Krill-Burger JM, Meyers RM, Ali L, Goodale A, Lee Y, Jiang G, Hsiao J, Gerath WFJ, Howell S, Merkel E, Ghandi M, et al. 2017. Defining a cancer dependency MAP. *Cell* **170**:564–576. DOI: <https://doi.org/10.1016/j.cell.2017.06.010>, PMID: 28753430
- Tyssowski KM**, DeStefino NR, Cho JH, Dunn CJ, Poston RG, Carty CE, Jones RD, Chang SM, Romeo P, Wurzelmann MK, Ward JM, Andermann ML, Saha RN, Dudek SM, Gray JM. 2018. Different neuronal activity patterns induce different gene expression programs. *Neuron* **98**:530–546. DOI: <https://doi.org/10.1016/j.neuron.2018.04.001>, PMID: 29681534

- Whyte WA**, Orlando DA, Hnisz D, Abraham BJ, Lin CY, Kagey MH, Rahl PB, Lee TI, Young RA. 2013. Master transcription factors and mediator establish super-enhancers at key cell identity genes. *Cell* **153**:307–319. DOI: <https://doi.org/10.1016/j.cell.2013.03.035>, PMID: 23582322
- Wiseman EF**, Chen X, Han N, Webber A, Ji Z, Sharrocks AD, Ang YS. 2015. Dereglulation of the foxm1 target gene network and its coregulatory partners in oesophageal adenocarcinoma. *Molecular Cancer* **14**:69. DOI: <https://doi.org/10.1186/s12943-015-0339-8>, PMID: 25889361
- Wu T**, Lyu R, You Q, He C. 2020. Kethoxal-assisted single-stranded DNA sequencing captures global transcription dynamics and enhancer activity in situ. *Nature Methods* **17**:515–523. DOI: <https://doi.org/10.1038/s41592-020-0797-9>, PMID: 32251394
- Yan W**, Chen D, Schumacher J, Durantini D, Engelhorn J, Chen M, Carles CC, Kaufmann K. 2019. Dynamic control of enhancer activity drives stage-specific gene expression during flower morphogenesis. *Nature Communications* **10**:1705. DOI: <https://doi.org/10.1038/s41467-019-09513-2>, PMID: 30979870
- Yang T**, Zhang F, Yardımcı GG, Song F, Hardison RC, Noble WS, Yue F, Li Q. 2017. HiCRep: assessing the reproducibility of hi-C data using a stratum-adjusted correlation coefficient. *Genome Research* **27**:1939–1949. DOI: <https://doi.org/10.1101/gr.220640.117>, PMID: 28855260
- Zhang Y**, Liu T, Meyer CA, Eeckhoutte J, Johnson DS, Bernstein BE, Nusbaum C, Myers RM, Brown M, Li W, Liu XS. 2008. Model-based analysis of chip-seq. *Genome Biology* **9**:R137. DOI: <https://doi.org/10.1186/gb-2008-9-9-r137>, PMID: 18798982
- Zhang Z**, Lee JH, Ruan H, Ye Y, Krakowiak J, Hu Q, Xiang Y, Gong J, Zhou B, Wang L, Lin C, Diao L, Mills GB, Li W, Han L. 2019. Transcriptional landscape and clinical utility of enhancer RNAs for ERα-targeted therapy in cancer. *Nature Communications* **10**:4562. DOI: <https://doi.org/10.1038/s41467-019-12543-5>, PMID: 31594934
- Zhao Y**, Wang L, Ren S, Wang L, Blackburn PR, McNulty MS, Gao X, Qiao M, Vessella RL, Kohli M, Zhang J, Karnes RJ, Tindall DJ, Kim Y, MacLeod R, Ekker SC, Kang T, Sun Y, Huang H. 2016. Activation of P-TEFb by androgen receptor-regulated enhancer RNAs in castration-resistant prostate cancer. *Cell Reports* **15**:599–610. DOI: <https://doi.org/10.1016/j.celrep.2016.03.038>, PMID: 27068475
- Zhao S**, Allis CD, Wang GG. 2021. The language of chromatin modification in human cancers. *Nature Reviews. Cancer* **21**:413–430. DOI: <https://doi.org/10.1038/s41568-021-00357-x>, PMID: 34002060
- Zhou Y**, Zhou B, Pache L, Chang M, Khodabakhshi AH, Tanaseichuk O, Benner C, Chanda SK. 2019. Metascape provides a biologist-oriented resource for the analysis of systems-level datasets. *Nature Communications* **10**:1523. DOI: <https://doi.org/10.1038/s41467-019-09234-6>, PMID: 30944313

## Appendix 1

## Appendix 1—key resources table

Reagent type (species) or resource	Designation	Source or reference	Identifiers	Additional information
Cell line ( <i>H. sapiens</i> )	OE19	ACACC	96071721	
Cell line ( <i>H. sapiens</i> )	CP-A	ATCC	KR-42421	
Cell line ( <i>H. sapiens</i> )	OE19-dCas9-KRAB	<b>Rogerson et al., 2020</b>		OE19 transfected with vector to express dCas9-KRAB under doxycycline control
Antibody	Rabbit monoclonal anti-Erk1/2 antibody	Cell Signalling Technology	4695S	(1:1000)
Antibody	Donkey polyclonal anti-mouse secondary antibody (800CW)	Licor	925-32,212	(1:10,000)
Antibody	Donkey polyclonal anti-rabbit secondary antibody (700CW)	Licor	925-32,213	(1:10,000)
Antibody	Mouse monoclonal anti-Cas9	Diagenode	C15200229	(1:10,000)
Antibody	Rabbit monoclonal anti-BRD4	Abcam	ab128874	0.5 µg/2-4 × 10 <sup>5</sup> cells
Antibody	Rabbit polyclonal anti-CTCF	Merck-Millipore	07-729	0.5 µg/2-4 × 10 <sup>5</sup> cells
Antibody	Rabbit polyclonal anti-H3K27ac	Abcam	ab4729	0.5 µg/2-4 × 10 <sup>5</sup> cells
Antibody	Mouse polyclonal anti-H3K27me3	Merck-Millipore	07-449	0.5 µg/2-4 × 10 <sup>5</sup> cells
Antibody	Rabbit polyclonal anti-H3K4me1	Abcam	ab8895	0.5 µg/2-4 × 10 <sup>5</sup> cells
Antibody	Rabbit polyclonal anti-H3K4me2	Diagenode	pAb-035-010	0.5 µg/2-4 × 10 <sup>5</sup> cells
Antibody	Rabbit polyclonal anti-H3K4me3	Abcam	ab8580	0.5 µg/2-4 × 10 <sup>5</sup> cells
Antibody	Rabbit polyclonal anti-H3K36me3	Diagenode	pAb-058-010	0.5 µg/2-4 × 10 <sup>5</sup> cells
Antibody	Mouse monoclonal anti-H4K20me1	Diagenode	mAb-147-010	0.5 µg/2-4 × 10 <sup>5</sup> cells
Antibody	Mouse monoclonal anti-PoII	Abcam	ab817	0.5 µg/2-4 × 10 <sup>5</sup> cells
Antibody	Rabbit polyclonal anti-PoII-S2	Abcam	ab5095	0.5 µg/2-4 × 10 <sup>5</sup> cells
Antibody	Rabbit polyclonal anti-PoII-S5	Abcam	ab5131	0.5 µg/2-4 × 10 <sup>5</sup> cells
Antibody	Rabbit polyclonal anti-Med1	<a href="https://www.antibodies.com/">https://www.antibodies.com/</a>	A98044/10 UG	0.5 µg/2-4 × 10 <sup>5</sup> cells
Recombinant DNA reagent	pGL3 reporter vector	Promega	E1761	
Recombinant DNA reagent	hSTARR_ORI vector	Addgene	99296	
Recombinant DNA reagent	pINDUCER20-GFP-AFOS	<b>Britton et al., 2017</b>		ADS5006
Recombinant DNA reagent	pCH110	Amersham		
Recombinant DNA reagent	pMD2.G	Addgene	12259	
Recombinant DNA reagent	psPAX2	Addgene	12260	
Sequence-based reagent	Primers	This study		Primers for amplification through PCR (See supplementary file). Primers can be ordered through any commercial vendor.
Commercial assay or kit	Lipofectamine RNAiMAX	Thermo Fisher	13778150	
Commercial assay or kit	Cell Line Nucleofector™ Kit V	Lonza	VCA-1003	Used on Amaxa Nucleofector II with program T-020
Commercial assay or kit	Dual-Light Luciferase & β-Galactosidase Reporter System	Thermo Fisher	T1003	
Commercial assay or kit	SuperScript VILO Master Mix	Thermo Fisher	11755250	
Commercial assay or kit	PureLink Genomic DNA Mini kit	Thermo Fisher	K182001	
Commercial assay or kit	HiFi assembly	NEB	E5520S	
Commercial assay or kit	QuantiTect SYBR Green RT-PCR Kit	Qiagen	204243	

Appendix 1 Continued on next page

## Appendix 1 Continued

Reagent type (species) or resource	Designation	Source or reference	Identifiers	Additional information
Commercial assay or kit	RNeasy Plus Mini Kit	Qiagen	74134	
Commercial assay or kit	RNase-free DNase set	Qiagen	79254	
Commercial assay or kit	Ampure XP beads	Beckman Coulter Agencourt	A63881	
Commercial assay or kit	TruSeq stranded RNA library kit v2	Illumina	RS-122-2001	
Commercial assay or kit	Nextera DNA library prep kit	Illumina	FC-121-1031	
Commercial assay or kit	Nextera Index kit	Illumina	FC-121-1012	
Commercial assay or kit	NEBNext high fidelity 2x PCR master mix	NEB	M0541	
Commercial assay or kit	DNA Clean and Concentrator	Zymo	D4013	
Commercial assay or kit	Polyfect	Qiagen	301107	
Commercial assay or kit	PEG-it	System Biosciences	LV810A-1	
Commercial assay or kit	Polybrene	EMD Millipore	TR-1003	
Chemical compound, drug	Doxycycline	Sigma-Aldrich	D3447	Used at final concentration of 100 ng/ml
Chemical compound, drug	N <sub>3</sub> -kethoxal	Gift from Chuan He		Used at 5 mM
Peptide, recombinant protein	RNase	Sigma	R4642	Used at 100 µg/ml
Peptide, recombinant protein	pA-Tn5	Epiccypher	15-1017	
Peptide, recombinant protein	EGF	Thermo Fisher	10450-013	5 µg/l
Peptide, recombinant protein	Bovine pituitary extract	Thermo Fisher	1E+07	Used at 50 mg/l
Software, algorithm	Trimmomatic	<b>Bolger et al., 2014</b>	V0.34	<a href="http://www.usadellab.org/cms/?page=trimmomatic">http://www.usadellab.org/cms/?page=trimmomatic</a>
Software, algorithm	ChromHMM	<b>Ernst and Kellis, 2012</b>		
Software, algorithm	Bowtie2	<b>Langmead and Salzberg, 2012</b>	v2.3.0	<a href="http://bowtie-bio.sourceforge.net/bowtie2/index.shtml">http://bowtie-bio.sourceforge.net/bowtie2/index.shtml</a>
Software, algorithm	STAR	<b>Dobin et al., 2013</b>	V2.5.4	<a href="https://github.com/alexdobin/STAR">https://github.com/alexdobin/STAR</a>
Software, algorithm	Mac2	<b>Zhang et al., 2008</b>	v2.1.1	<a href="https://github.com/taoliu/MACS">https://github.com/taoliu/MACS</a>
Software, algorithm	DESeq2	<b>Love et al., 2014</b>	V1.22.2	<a href="https://bioconductor.org/packages/release/bioc/html/DESeq2.html">https://bioconductor.org/packages/release/bioc/html/DESeq2.html</a>
Software, algorithm	TOBIAS	<b>Bentsen et al., 2020</b>	v0.5.1	<a href="https://github.com/loosolab/TOBIAS">https://github.com/loosolab/TOBIAS</a>
Software, algorithm	featureCounts	<b>Liao et al., 2014</b>	V1.6.2	<a href="http://subread.sourceforge.net">http://subread.sourceforge.net</a>
Software, algorithm	FastQC		v0.11.4	<a href="https://www.bioinformatics.babraham.ac.uk/projects/fastqc/">https://www.bioinformatics.babraham.ac.uk/projects/fastqc/</a>
Software, algorithm	bedtools	<b>Quinlan and Hall, 2010</b>	v2.26.0	<a href="https://bedtools.readthedocs.io/en/latest/">https://bedtools.readthedocs.io/en/latest/</a>
Software, algorithm	DeepTools	<b>Ramírez et al., 2016</b>	V2.5.0	<a href="https://deeptools.readthedocs.io/en/develop/">https://deeptools.readthedocs.io/en/develop/</a>
Software, algorithm	Metascape	<b>Zhou et al., 2019</b>		<a href="https://metascape.org/gp/index.html">https://metascape.org/gp/index.html</a>
Software, algorithm	Homer	<b>Heinz et al., 2010</b>	v4.9	<a href="http://homer.ucsd.edu/homer/">http://homer.ucsd.edu/homer/</a>
Software, algorithm	R	<b>R Development Core Team, 2018</b>	v3.5.1	<a href="https://www.r-project.org/">https://www.r-project.org/</a>
Software, algorithm	GraphPad Prism		V8.0	<a href="https://www.graphpad.com/">https://www.graphpad.com/</a>
Software, algorithm	Morpheus	Broad Institute		<a href="https://software.broadinstitute.org/morpheus/">https://software.broadinstitute.org/morpheus/</a>
Other	Crystal violet	Sigma-Aldrich	HT90132	Histological DNA stain. Used at concentration of 0.1%
Other	Gibco RPMI 1640	Thermo Fisher	52400	Cell culture medium for OE19s.

Appendix 1 Continued on next page

## Appendix 1 Continued

Reagent type (species) or resource	Designation	Source or reference	Identifiers	Additional information
Other	Gibco fetal bovine serum	Thermo Fisher	10270	Cell culture supplement.
Other	Gibco penicillin/streptomycin	Thermo Fisher	15140122	Cell culture supplement
Other	Keratinocyte SFM (1×)	Thermo Fisher	17005042	Cell culture medium for CP-As.